Chapter 6

Manganese Sulfide (MnS) Nanocrystals: Synthesis, Properties, and Applications

Anna M. Ferretti, Sara Mondini and
Alessandro Ponti

Additional information is available at the end of the chapter

http://dx.doi.org/10.5772/65092

Abstract

Manganese(II) sulfide (MnS) is an interesting material for both fundamental and applicative research, especially when its bulk properties are modulated by reducing the size into the nanometric region (< 100 nm). Due to its polymorphism, MnS is an attractive material to develop synthetic strategies for polymorphism control. We have reviewed the literature concerning MnS nanosystems having at least one dimension smaller than 100 nm. Successful synthetic techniques for the preparation of zero- and one-dimensional MnS nanosystems (either homogeneous and heterogeneous) with size, shape, and polymorphism control are presented with emphasis on solvothermal techniques and on studies devoted to understanding the growth mechanism and the polymorphism. Properties and applications are collected in three broad areas corresponding to nanosize MnS used as an optical, electric, and magnetic material. MnS has attracting properties such as its large bandgap, which makes it promising for emission in the ultraviolet region. The magnetic properties have also arisen attention since MnS is antiferromagnetic at low temperature and (super)paramagnetic at room temperature. Finally, the layered structure of the hexagonal polymorph is responsible for the good performance of nanosize MnS as a lithium-ion battery electrode or supercapacitor material since the insertion/exchange of small ions is easy.

Keywords: manganese sulfide, MnS, nanocrystal, one-dimensional nanostructure, polymorphism control, solvothermal synthesis

1. Introduction

Manganese(II) sulfide (MnS) is a p-type semiconductor with a wide bandgap (E_g = ~3 eV) [1] that undergoes a transition to an antiferromagnetically (AFM) ordered phase below room temperature [2]. These features attracted interest for the potential applications of nanosized MnS in the field of short wavelength optoelectronics [3–5], or as a photoluminescent component [6], photoreduction catalysts [7], and contrast agent for magnetic resonance imaging (MRI) [8, 9]. The optical properties of MnS have also raised considerable interest in protobiology since it is deemed to have played a key role (along with ZnS in mixed haloes formed around primeval sub-aerial hot springs) in the prebiotic photosynthesis development, thanks to its ability to photoreduce CO_2 [7]. More recently, interesting energy-related applications have been demonstrated, where MnS was employed as an electrode material in Li-ion batteries [10–13] and as a supercapacitor material [14, 15]. These interesting properties and promising applications have raised considerable attention and research on small MnS particles can be considered to begin with the submission of three papers within the middle 6 months of 2001. In March, the revised version of a paper by Qian and coworkers [16] describing the synthesis of submicrometric particles of all three polymorphs of MnS was submitted and appeared in print later that year. Truly nanometric (<100 nm) MnS nanocrystals (NCs) were independently reported by Banin and Cheon research groups in 2001. It is noteworthy that the paper by Cheon and coworkers [17] was received by the publisher just 2 weeks before the paper by Banin and coworkers [18] arrived at a different publisher. However, the latter article appeared in print in 2001 while the former in 2002.

Three polymorphs (α, β, and γ) of MnS are known, and their crystal structure is represented in **Figure 1**. In the cubic rock-salt α-MnS structure, sulfide anions an expanded fcc lattice, and the manganese cations occupy all octahedral sites. The metastable form β-MnS has the cubic zincblende structure. Similarly to α-MnS, β-MnS comprises an expanded fcc lattice of S^{2-}anions, but in this polymorph, the Mn^{2+} cations reside on half of the tetrahedral sites. Finally, γ-MnS has the hexagonal wurtzite structure, based on a slightly compressed (c/a = 1.618) hcp lattice of sulfide anions with manganese cations occupying half of the tetrahedral sites. The polymorphs have similar but unequal physical properties; for instance, all the three forms of MnS undergo transition to an AFM ordered structure [19], but the transition temperature varies from T_N ~80 K for γ-MnS to ~100 K for β-MnS and 154 K for α-MnS [2]. The magnetic structures below T_N were determined by neutron diffraction and could be explained by the interplay between the crystal structure and the superexchange interaction between the magnetic Mn^{2+} cations [19]. α-MnS displays the well-known Type-II structure where the magnetic moments are ferromagnetically (FM) coupled within the (111) planes and successive (111) planes form an AFM structure. Both β- and γ-MnS display Type-III ordering since in these structures the Mn^{2+} ions are coordinated tetrahedrally. For the details of these more complicated magnetic structures refer to Reference [19].

Naturally occurring MnS minerals with α, β, and γ structures are known, but they have curiously been discovered in a large time interval. Natural α-MnS has been known as alabandite since the beginning of the nineteenth century [20] and is a widespread manganese ore.

http://dx.doi.org/10.5772/65092

MnS minerals with β and γ structures have been much more recently reported upon: rambergite (γ-MnS) has been discovered in 1996 in Sweden [21] whereas browneite (β-MnS) was found in a meteorite collected in Poland in 2012 [22].

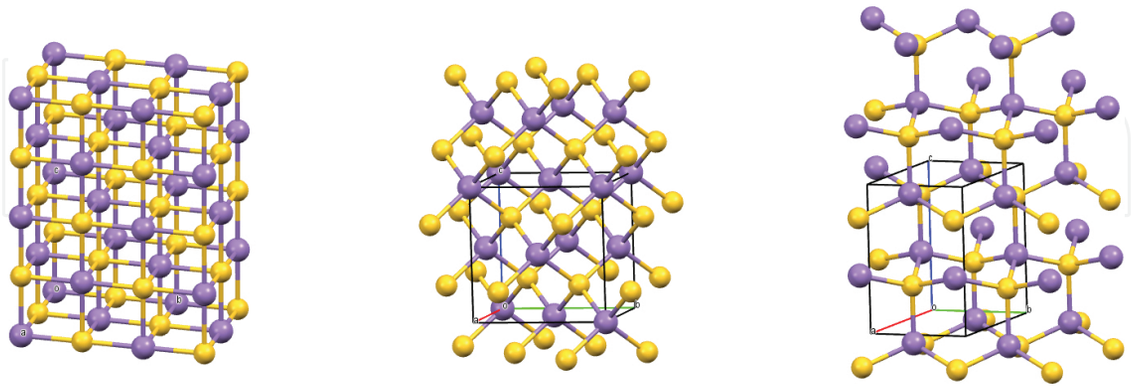

Figure 1. Crystal structure of the three polymorphs of MnS. Left: cubic α-MnS (rock salt); middle: cubic β-MnS (zinc-blende); right: hexagonal γ-MnS (wurtzite). The primitive cell is also shown. Color code: Mn, violet; S, yellow.

We limit our review to homogeneous or heterogeneous nanostructures that comprise pure MnS with at least one dimension smaller than 100 nm (some MnS sub-microcrystals are included when of particular interest). Both zero- (0D) and one-dimensional (1D) MnS nanosystems have been prepared using several bottom-up methods ranging from solvothermal and hydrothermal "wet" techniques to chemical vapor deposition (CVD). Though we will review MnS nanostructures prepared by any technique, we will give some detail of solvothermal methods, which found the most widespread application in the synthesis of 0D nanostructures and show a nice diversity in the choice of precursors and experimental conditions. Conversely, 1D nanosystems (rods, wires, saws) were often obtained prepared by the CVD. Some heterostructures, both 0D and 1D, comprising MnS have also been prepared by solvothermal or CVD techniques and displayed peculiar properties. The issue of polymorphism control in 0D NCs has been the subject of several reports showing that both physical and chemical parameters can be used to obtain the desired crystal structure.

2. Synthesis and characterization

In this section, we will review both the synthetic methods for the preparation of zero-dimensional (0D) and one-dimensional (1D) MnS nanosystems and their morphological [usually performed resorted to scanning electron microscopy (SEM) and transmission electron microscopy (TEM)], structural [X-ray (XRD) and electron (ED) diffraction], and compositional [usually by energy dispersive X-ray spectroscopy (EDX, a.k.a. EDS), more rarely by electron energy loss spectroscopy (EELS) and its imaging counterpart electron spectroscopy imaging (ESI)] characterization. The optical, electric, and magnetic properties of the MnS nanosystems will be discussed in the following sections. The present section will separately deal with 0D and 1D MnS nanostructures, and the reports specifically addressing the control of the MnS

polymorphism are collected at the end of the section. Synthetic studies involving systematic variation in the reaction conditions are deemed particularly interesting and will be given particular attention.

2.1. Zero-dimensional (0D) nanosystems

In this subsection, we focus on nanostructures comprising MnS NCs with aspect ratio close to 1 and start with chemically homogeneous nanosystems, i.e., pure MnS NCs. The subsection is concluded by reviewing heterogeneous nanosystems comprising a 0D MnS NC.

2.1.1. Homogeneous nanocrystals

Of course, most examples of 0D nanosystems are homogeneous MnS NCs or a mixture of two or three polymorphic MnS NCs. We separately review NCs obtained by solvothermal techniques, that is, where one or more precursors are decomposed at high temperature in non-aqueous solvent in an inert atmosphere, possibly in the presence of other compounds acting as a growth regulator, protective coating, shape- or polymorph-inducer, etc.

2.1.1.1. Solvothermal methods

To the best of our knowledge, the synthesis of 0D MnS NCs with at least one dimension below 100 nm was independently reported by two research groups in 2001. It is noteworthy that one paper was received by the publisher just 2 weeks before the other one arrived at a different publisher. However, the latter article appeared in print in 2001 while the former in 2002. In the presented by Banin group, α-MnS NCs were obtained using a solvothermal technique employing reagents rarely found in subsequent work [18]. The procedure involved the injection of a trioctylphosphine/trioctylphosphine oxide (TOP/TOPO) solution of *both* precursors $MnCl_2$ and $(Me_3Si)_2S$ (Mn:S = 1:0.67 to 1:0.77, defect of S) in hot TOPO (360°C). Size control was achieved by varying the concentration of Mn from 0.066 to 0.13 and 0.2 M, so that 80, 40, and 20 nm nanosystems were obtained. XRD showed that the product was pure α-MnS NCs, but the crystallite size turned out to be 12 nm. This result and the grainy appearance of the TEM images suggest that the nanosystems are different-sized agglomerates of smaller MnS crystallites. The first magnetic characterization of MnS NCs was also reported. The paper presented by the Cheon group [17] describes 0D α-MnS NCs and "composite" β-MnS/γ-MnS nanowires and multipodes obtained by a very different solvothermal protocol. It involved a single precursor, manganese bis(*N*,*N*-diethylcarbamate) $Mn(Et_2N\text{-}CS_2)_2$ (Mn:S = 1:4), which was dissolved in hexadecylamine, then injected into hot hexadecylamine and aged for 20 min. By varying the reaction temperature, the MnS NCs shape and crystal structure could be controlled, but not independently. At 120°C, γ-MnS nanowires and γ-MnS multipodes with the β-MnS core were obtained whereas ~30 nm α-MnS nanocubes were produced at 250°C. In subsequent research, it has often been confirmed that low/high reaction temperature favors the (β, γ)/α crystal structure, as expected on the basis of the relative thermodynamic stability. The first optical characterization of MnS NCs was also reported.

http://dx.doi.org/10.5772/65092

Using a single molecule as a precursor for both Mn and S could offer a few advantages, e.g., Mn–S bonds are already present and likely to survive the precursor decomposition, and the Mn:S molar ratio is exactly fixed. Moreover, precursor synthesis is usually easy. Thus, several papers reported the use of a single precursor, often chemically similar to $Mn(Et_2N\text{-}CS_2)_2$, for the preparation of MnS NCs. In a paper regarding the synthesis of NCs of many divalent metal sulfides [23], manganese *O*-hexadecylxanthate $Mn(C_{16}H_{33}O\text{-}CS_2)_2$ (Mn:S = 1:4) was used to obtain α-MnS NCs. The morphology is irregular and no size information was given. The authors noted that the precursor is easily attacked by hexadecylamine at room temperature, so that trioctylamine had to be employed as a reaction solvent at 150°C. In the last example [24] involving a single precursor, $Mn(Ph\text{-}COS)_2$TMEDA (Mn:S = 1:2, Ph-COS = thiobenzoate, TMEDA = *N*,*N*,*N*′,*N*′-tetramethylethylenediamine), the roles of solvent and ligand are separated when non-coordinating 1-octadecene was used as a solvent while oleylamine was used as a ligand (TMEDA could also act as a Mn ligand). Octahedral NCs (size ca. 24 nm) were obtained by heating the precursor solution at 300–350°C for 2 h. XRD data showed pure α-MnS, as expected on the basis of the high reaction temperature, and EDX data confirmed the MnS stoichiometry. Single molecule precursors were also used to synthesize MnS NCs within mesoporous silica [25] (see Section 2.1.1.2), to study polymorphism control [26] (see Section 2.3), and to prepare β-MnS nanowires [27] (see Section 2.2.2).

The fixed Mn:S ratio inherent to the use of single-molecule precursors might also be regarded as a limitation while exploring synthetic conditions. This consideration, and the effort saved when precursors are commercially available, prompted many groups to employ a two-precursor strategy to synthesize MnS NCs. Of course, in this case, more care should be taken since the chemistry is more complex: the Mn–S bond has yet to be established and the reactive Mn and S species must be simultaneously present in the reaction environment. A convenient sulfide precursor is elemental sulfur (yellow powder, S_8), which is readily soluble in apolar solvents. The octameric molecule must be converted to sulfide S^{2-} anions during the reaction. Both 1-octadecene [28] and long-chain primary amines [29] have been shown to be able to produce the reactive sulfur species leading to metal sulfide NCs. MnS NCs were synthesized by heating an oleylamine solution of sulfur powder and $MnCl_2$ [30]. NC size and shape were varied by changing the Mn:S molar ratio. Nanorods with low aspect ratio (20 × 37 nm) were obtained using Mn:S = 1:1 at 240°C while long (17 × 44 nm) and short (23 × 37 nm) bullet-shaped NCs were synthesized using Mn:S = 2:1 and 3:1, respectively, at 280°C. Unfortunately, the NC composition and crystal structure seem to be not provided.

Sulfur can be inactivated when a long-chain carboxylic acid RCOOH is present in the reaction mixture, presumably due to the formation of RCOSH species [31]. It was shown that, in order to produce pure MnS NCs, the molar ratio Mn:S ≥ (Mn:RCOOH + 1) is required, e.g., if 1 equivalent of RCOOH is present, at least 2 equivalents of S are required (see **Figure 2**).

The synthesis of octahedral MnS NCs using a solvothermal protocol involving heating a solution of manganese carboxylate and sulfur powder in 1-octadecene has been studied in detail in Ref. [32]. Three manganese precursors were synthesized: Mn(II) distearate ($MnSt_2$), dioleate ($MnOl_2$), and hydroxyoleate [Mn(OH)(Ol)]. Whenever Mn:S ≥ 2, XRD showed that the produced NCs had α-MnS structure. Rietveld analysis of XRD profiles yielded NC size in

agreement with TEM data, thus showing that the NCs are single crystals. The NC size could be finely controlled by changing the precursor and the reaction temperature and time. Larger size is achieved by using $Mn(Ol)_2$ at higher temperature with longer reaction time . In this manner, α-MnS NCs with a size from 9.3 to 29.5 nm (and 10 other intermediate sizes) could be obtained (see **Figure 3**). The size dispersion was also investigated and it was interestingly found that $MnOl_2$ and Mn(OH)(Ol) behave oppositely. Size dispersion is minimum and maximum at 300°C for $MnOl_2$ and Mn(OH)(Ol), respectively. Furthermore, the change in size dispersion when the reaction time is varied is decreasing for $MnOl_2$ and volcano-shaped for Mn(OH)(Ol).

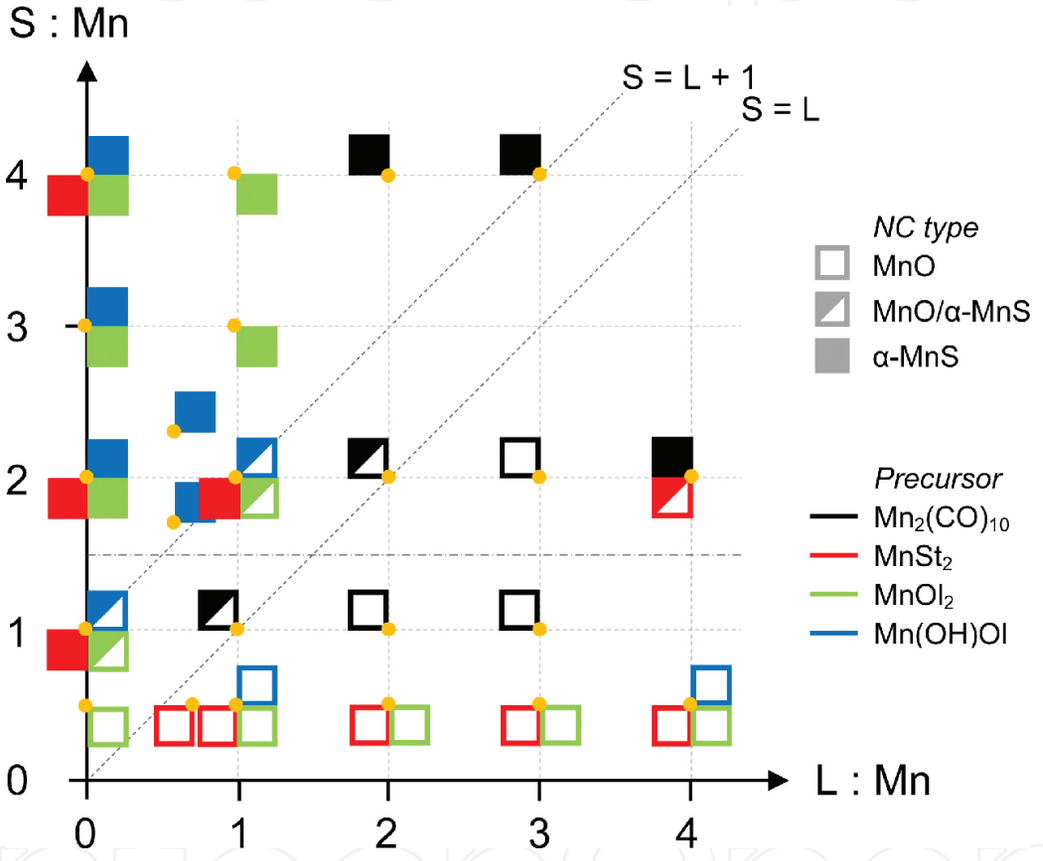

Figure 2. Synthetic outcome from solvothermal synthesis using different Mn precursors as a function of the L:Mn (L = surfactant) and S:Mn molar ratios. The type of NC is encoded as follows: open squares: MnO NCs; half-filled squares: mixture of MnO and α-MnS NCs; solid squares: α-MnS NCs. The precursors are color coded as follows. Black: $Mn_2(CO)_{10}$, red: $MnSt_2$, green: $MnOl_2$, blue: Mn(OH)Ol. The free surfactant, L, was stearic acid for $Mn_2(CO)_{10}$ and Mn distearate, and oleic acid for Mn dioleate and Mn hydroxyl oleate, respectively. Reprinted from Ref. [31] under the terms of the Creative Commons Attribution License.

$MnOl_2$ and sulfur powder were also used to prepare α-MnS NCs with a peculiar stellated-octahedral shape [33]. When a solution of $MnOl_2$ and S (1:2) in 1-octadecene was heated at 300°C, 15 nm spherical α-MnS NCs were obtained, but when a 1:1 v/v mixture of oleic acid and oleylamine was present in the reaction mixture, 45 nm α-MnS NCs with stellated-octahedral shape were produced. High-resolution TEM (HRTEM) and ED experiments showed that the latter are single crystals with elongated branches pointing along the six <001>

http://dx.doi.org/10.5772/65092

equivalent directions. A further solvothermal procedure involving sulfur powder and Mn(II) nitrate [34] can be found in Section 2.3; elemental S (and Mn) was also used in a hydrothermal protocol for α-MnS nanorods [35].

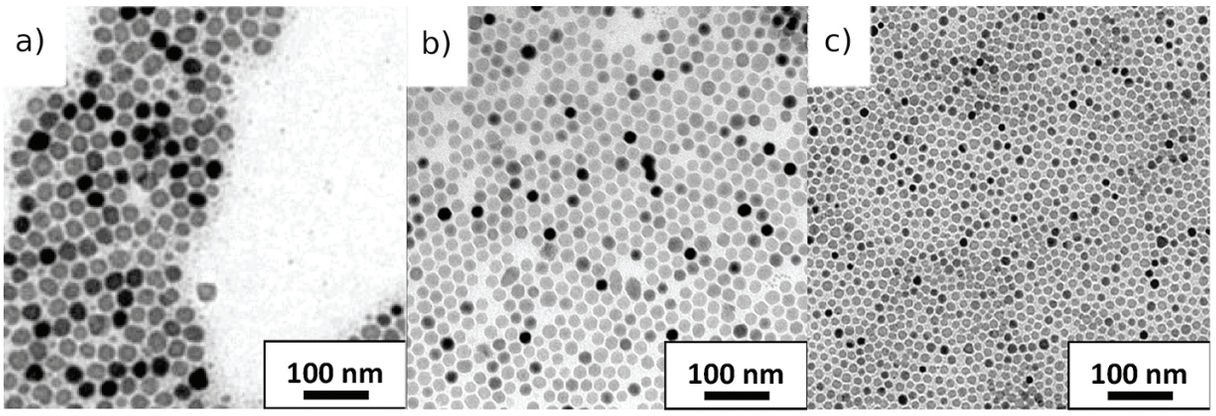

Figure 3. α-MnS NCs by a solvothermal method using sulfur powder in 1-octadecene. (a) 30 nm α-MnS NCs obtained using $Mn(Ol)_2$ as a metal precursor at 300°C. (b) 21 nm α-MnS NCs obtained using $Mn(Ol)_2$ at 320°C. (c) 14 nm α-MnS NCs obtained using Mn(OH)(Ol) at 300°C. Adapted from Puglisi A, Mondini S, Cenedese S, Ferretti AM, Santo N, Ponti A. Chem Mater. 2010;**22**:2804–2813. Ref. [32] Copyright (2010) American Chemical Society.

Since yellow sulfur powder (S_8) must be converted to sulfide anion S^{2-} during the formation of MnS NCs, using an inorganic sulfide as a precursor seemed appealing. In this manner, the synthesis of MnS NCs would not rely on the complex redox chemistry to produce sulfide anions from elemental sulfur. For instance, hydrated sodium sulfide has been employed in the synthesis of ZnS@MnS@ZnS heterostructures by co-precipitation with metal acetates in a hydroalcoholic medium (see Section 2.1.2) [6]. However, inorganic sulfides are poorly soluble in apolar solvents, which limits their application in solvothermal synthesis. This problem can be resolved by using ammonium sulfide $(NH_4)_2S$, which can be dissolved into dry oleylamine with a concentration of up to 0.5 M [36]. By injecting such solution into hot oleylamine solutions of metal precursors, the authors succeeded in the synthesis of NCs of several metal sulfides, including MnS. In this case, the sulfide (0.92 mmol) solution was injected into a solution of $MnCl_2$ (0.44 mmol, Mn:S = 1:2.1) in a 1:6 v/v (oleic acid)/oleylamine mixture at 250°C and aged for 5 min. Trapezoid-shaped MnS NCs with an average size of ca. 20 × 12 nm were obtained. The crystal structure was claimed to be γ; no further characterization data were provided. In a later report [13], a closely related reaction gave ca. 14 nm MnS NCs with trapezoid shape. In this case, the crystal structure was claimed to be β. This is surprising since the second reaction is just scaled up by a factor 2, the other synthetic conditions being unchanged. Re-examination of the XRD plots, especially the peak intensities, led us to the conclusion that both reactions produced a mixture of β- and γ-MnS NCs. In the first reaction, γ-MnS NCs were predominant and the reverse was true for the second reaction. The predominantly β-MnS NCs were then investigated as an electrode material for batteries (see below).

Another class of sulfide precursors, which can be considered as an intermediate between the extremes of elemental sulfur and inorganic sulfides, comprises small, typically organic, sulfur-

containing molecules that can easily release sulfide anions upon hydrolysis. Sodium thiocyanate was used for the synthesis of α-MnS nanobelts [37] (see below) and thiourea $(NH_2)_2C=S$ proved to be useful in hydrothermal protocols for the preparation of 1D MnS nanosystems [38, 39] (see below). In the context of the solvothermal synthesis of 0D MnS NCs, thioacetamide $CH_3C(S)\text{-}NH_2$ gave significant results. In a heat-up approach, involving heating at 250°C a solution of $MnCl_2$ (0.50 mmol) and thioacetamide (0.50 mmol, Mn:S = 1:1) in a 1:5 v/v (oleic acid)/oleylamine mixture, monodisperse α-MnS nanocubes were synthesized [52]. Size control was achieved by varying the reaction time. A cube edge size of 14 ± 1, 26 ± 2, and 40 ± 3 nm was obtained when the reaction mixture was heated for 30, 60, and 120 min, respectively; note that the size dispersion (mean/std.dev.) is nearly constant. EDX showed that Mn:S = 1:0.9 and the two elements are homogeneously distributed. Based on the reaction carried out at different temperatures, the authors proposed that nanocubes formed via the oriented aggregation of very small spherical NCs followed by intraparticle ripening. It is interesting to note that the final nanocubes also spontaneously form meta-crystals with the simple cubic packing driven by strong interactions between the {001} faces of the nanocubes. Yang et al. [40] used thiourea in their investigation aimed at understanding the effect of reaction temperature and pressure on the crystal structure of MnS nanosystems (see Section 2.3). NC aggregation was also observed in another synthetic example where thiourea was used as a precursor [9]. In this case, $MnCl_2$ (0.20 mmol) and thioacetamide (0.60 mmol, Mn:S = 1:3) were dissolved in a complex mixture of 1-octanol/octylamine/(oleic acid)/acetone 3:3:3:1 v/v and autoclaved at 150°C for 1 h. The product comprised large (ca. 90 nm) spherical aggregates of small (ca. 5 nm) α-MnS NCs. The authors claim that NC aggregation is induced by water generated by the decomposition of thioacetamide, but it should be noted that the hydrolysis of thioacetamide to acetamide and H_2S consumes (not produces) water. Interestingly, when the hexane dispersion of these α-MnS NC aggregates was shaken with an aqueous sodium citrate solution at 85°C, the aggregates could be separated and the individual α-MnS NCs became water dispersible. These NCs were next investigated as a possible MRI contrast agent (see below).

To conclude this subsection, we mention an interesting report describing how γ-MnS NCs can be produced by cation exchange from $Cu_{2-x}S$ NCs thanks to the similarity of the roxbyite and wurtzite crystal structures [41]. Disk-shaped (ca. 6 × 16 nm) $Cu_{2-x}S$ NCs suspended in TOP were injected into a solution of Mn chloride tetrahydrate in an oleylamine/toluene mixture at 100°C and reacted for 10 min before cooling. The NCs retained their size and shape. Despite EDX showed about 10% residual Cu, both XRD and ED displayed a pure γ-MnS pattern. The interesting point is that, starting from the roxbyite structure (distorted hcp lattice of sulfide anions with copper cations in tetrahedral and trigonal sites), γ-MnS NCs with wurtzite structure (hcp lattice of S^{2-} anions with Mn^{2+} cations in tetrahedral sites) were only obtained. Since both α- and β-MnS have a ccp lattice of S^{2-} anions, the authors could conclude that cation exchange preserved the compact sulfide lattice, as expected. However, the comparison of these experiments with cation exchange assays using cobalt showed that also the cation site occupation (tetrahedral *vs*. octahedral) was preserved.

2.1.1.2. Other methods

A few examples reporting non-solvothermal synthesis of 0D MnS NCs could be found. Sub-microcystals of all three MnS polymorphs were prepared by a hydrothermal method [42]. Since this report describes in detail how to control the crystal structure of the product, it is reviewed in Section 2.3. Hydrothermal methods were used to synthesize 1D MnS NCs, as reviewed in the next section.

Another method used to synthesize 0D MnS NCs involves the growth of the NCs within the pores of mesoporous silica, thanks to heat or chemical treatment following impregnation of the porous materials. Spherical γ-MnS NCs were synthesized inside the pores of MCM-41 or SBA-15 silica host material [43]. It should be noted that the authors used the old nomenclature (e.g., see Ref. [19]) and denominated γ-MnS as "wurtzite β-MnS". Unfortunately, for synthetic and morphological details, the reader is referred to a previous publication [44], which describes the synthesis of Mn-doped ZnS NCs. We then provide synthetic and morphological data with this *caveat* in mind. Mesoporous silica was impregnated with Mn(II) acetate and, after drying, treated with H_2S gas at 100°C for 24 h. The impregnation/reaction cycle was carried out two or three times. The porous structure of the host material was not affected by these treatments. Using such moderate temperature for the chemical treatment, reaction with the silica wall and formation of other MnS polymorphs could be avoided. γ-MnS NCs were obtained with diameter 3, 6, 8, and 11 nm employing silica with different pore sizes.

A similar method was used to synthesize MnS NCs within mesoporous silica [25]. The main differences are the use of $Mn(EtO\text{-}CS_2)_2TMEDA$ as a xanthate single precursor with Mn:S = 1:4 and the heat (instead of chemical) treatment of the impregnated silica. As we will soon see, this causes large difference in the outcome. The P123 mesoporous silica (pore diameter 7 nm) impregnated with $Mn(EtO\text{-}CS_2)_2TMEDA$ was dried and heated in a N_2 atmosphere at 450°C for 12 h. In this case also, the ordered porous morphology of the host material was unchanged after the heat treatment. EDX showed that the products had Mn:S = 1:1 stoichiometry, but in contrast to the previous case, the XRD pattern contained peaks from all three MnS polymorphs. XRD data estimated that the MnS NC size ranged between 3.5 and 5.1 nm, smaller than the pore diameter. In this case, the influence of the mesoporous environment on the reaction mechanism was such that NCs with α, β, and γ structures were obtained, as supported by the fact that, in the absence of P123 silica, the heat treatment of $Mn(EtO\text{-}CS_2)_2TMEDA$ gave 200 nm MnS NCs with purely zinc blend β structure.

2.1.2. Heterostructures

A few examples of 0D heterostructured nanosystems including a MnS component have been reported, mostly related to optical applications. Nanosystems including both MnS and ZnS have gathered some attention thanks to the isostructurality of ZnS (zincblende, $F\bar{4}3m$, a = 0.54 nm) and β-MnS (a = 0.56 nm) and the similar cell size. MnS@ZnS nanosystems were prepared by a two-step solvothermal method [45]. The MnS core NCs were synthesized by injecting a sulfur solution in 1-octadecene (1.2 mmol of S) into a hot (270°C) solution of Mn(II) stearate (0.048 mmol, Mn:S = 1:25) and rapidly cooling the mixture. MnS NCs isolated after this first

step are very small (diameter 2.3 nm). The ZnS shell was prepared by re-heating the MnS cores at 250°C and there injecting varying amounts of Zn(II) stearate. These nanosystems were subjected to a detailed investigation of their optical properties, but other characterization data are not abundant. The MnS@ZnS heterostructures have a diameter ranging from 4.2 to 6.0 nm, so that the ZnS shell thickness can be estimated to be in the 0.9–1.8 nm interval. The HRTEM and ED data of 5.4 nm MnS@ZnS nanosystems suggest that the MnS core has the β structure. This was confirmed in a later article by the same group [46], at least for the naked MnS NCs, by means of XRD. Recall that isostructural ZnS and β-MnS have cell size differing by about 0.7%, so that the XRD patterns of nanosized ZnS and β-MnS cannot be discerned. The detailed optical investigation of these systems is reviewed below.

Aiming at improving the optical properties of these MnS@ZnS nanosystems, ZnS@MnS@ZnS heterostructures were synthesized by a three-step hydroalcoholic co-precipitation protocol [6]. To a solution of Zn(II) acetate dihydrate (25 mmol) in an ethanol/water 1:1 mixture, a hydroalcoholic solution of Na_2S (25 mmol) was added dropwise and a white precipitate formed. Next, a hydroalcoholic solution of Mn(II) acetate tetrahydrate (5–20 mmol) was added to form the intermediate MnS layer. Finally, the ZnS shell was prepared by a similar procedure involving the addition of 12.5 mmol of Zn followed by 25 mmol of S. Again, a detailed optical investigation (see below) came with limited morphostructural characterization. The XRD pattern of the ZnS@MnS@ZnS heterostructures is very close to that of the ZnS cores, suggesting that the MnS layer could be amorphous or β-MnS, which is isostructural with ZnS. The nanosystem size calculated from the XRD data is in agreement with that obtained from TEM images, i.e., the ZnS core has a diameter of 6.5 nm and the ZnS@MnS@ZnS nanosystems range from 5.5 to 6.3 nm, showing that leaching occurs in the second/third step. Note that no sulfur is added in the second synthetic step, thus suggesting that Mn diffuses into the lattice of the ZnS core, as also supported by optical measurements.

Finally, $Cu_{1.94}S$/γ-MnS heterostructures have been solvothermally synthesized and subjected to a detailed structural investigation [50]. The solvothermal protocol comprises two steps: first, $Cu_{1.94}S$ NCs are formed by heating a solution of anhydrous Cu(II) acetate (0.31 mmol) in a 1:2 v/v mixture of oleylamine and dodecanethiol at 220°C for 15 min, the latter one also acts as a sulfur source. Then, anhydrous Mn(II) acetate (0.70 mmol) dissolved in oleylamine is injected into the hot mixture. After aging for further 10–20 min, the mixture was cooled and the nanosystems isolated. When no Mn is added, one recovers $Cu_{1.94}S$ NCs with monoclinic structure and disk shape (diameter ~15 nm, height ~7 nm). The flat disk surfaces correspond to the (800) planes of the monoclinic structure. When the second synthetic step is carried out, it turns out that γ-MnS nanocylinders heteroepitaxially grew on *one* of the $Cu_{1.94}S$ nanodisk flat surfaces. The γ-MnS nanocylinder has the same diameter as the $Cu_{1.94}S$ nanodisk and is 14, 16, and 21 nm long for 10, 15, 20 min aging time, respectively. It is interesting that the thickness of the $Cu_{1.94}S$ nanodisk reduced to ~4 nm. HRTEM images show that both components are single crystals and that the interface, where $Cu_{1.94}S$ (800) and γ-MnS (001) planes face each other, is very abrupt. HRTEM images clearly show that the (101) planes of γ-MnS smoothly connect with the (442) planes of $Cu_{1.94}S$ across the interface, the interplanar mismatch being very small (0.3%). The authors proposed that the heterostructure initially forms by cation

exchange, favored by the presence of a hcp lattice of sulfide anions in both crystals and, perhaps, by the fact that Cu^{+} and Mn^{2+} ions occupy different sites in the S^{2-} lattice. However, the question why γ-MnS grows on *one* nanodisk side only remains open.

2.2. One-dimensional (1D) nanosystems

Most 1D MnS nanowires (high aspect ratio) have been synthesized by CVD, a technique involving the decomposition of volatile thermally-labile precursors on a substrate thus producing very pure, thin-film, possibly nanostructured coatings. Because of the spatially anisotropic synthetic environment, CVD is apt for inducing the growth of 1D nanosystems. However, examples of 1D MnS nanosystems prepared by solvothermal techniques could also be found, usually nanorods with a lower aspect ratio than nanowires. Regarding the product crystal structure, 1D nanosystems crystallized in the γ-MnS structure, which is prone to anisotropic growth having hexagonal (uniaxial) structure, and in the cubic α-MnS structure. We could not find examples of β-MnS 1D nanosystems.

2.2.1. Nanobelts, nanorods, and nanosaws

We start with the notable example of α-MnS nanobelts synthesized by a solvothermal method. Indeed, it is noteworthy that 1D nanosystems were obtained notwithstanding that both the crystal structure and the synthetic environment are isotropic. The preparation of α-MnS nanobelts [37] involved dissolving Mn(II) acetate tetrahydrate (1 mmol) and ammonium thiocyanate (2 mmol, Mn:S = 1:2) in molten dodecylamine (40 ml) and autoclaving this solution for 72 h at 220°C. XRD showed that the product is pure α-MnS. As observed by SEM, the product comprises belt-like nanostructures, several μm long and 50–150 nm wide with an estimated thickness of 25 nm. The nanobelts have constant width along their entire length. TEM confirmed the nanobelt morphology and on the basis of ED data, the authors claimed that the nanobelt growth direction is [100] but the presented data are also consistent with the [110] growth (actually with growth along any [*hk*0] direction). The authors interestingly explored how the outcome depends on the synthetic conditions. Upon changing reaction time or temperature, the quality of the nanobelts was poor. When Mn(II) chloride or sulfate was used, the obtained product was bulk α-MnS. Replacing ammonium thiocyanate with sulfur powder or thioacetamide yielded α-MnS nanocubes and the latter were also obtained when dodecylamine was substituted with diluted ammonia. Use of sodium sulfide gave α-MnS microcrystals. It is clear that formation of the nanobelts critically depends on both physical and chemical synthetic conditions. The authors proposed that at least three conditions must be met for the formation of α-MnS nanobelts: temperature higher than 200°C to form the α-MnS phase, slow nucleation and growth (here obtained thanks to the slow release of sulfur from thiocyanate and the coordination of Mn(II) by dodecylamine), and selective surfactant adsorption on the different crystal faces of MnS. We also note that adsorption of acetate anions on the NC surface seems to be important as Mn(II) chloride or sulfate gave bulk α-MnS. The question whether α-MnS nanobelts originate from γ-MnS 1D nanostructures by a phase transformation remains open though one should note that the peculiar nanobelt morphology has not been observed in γ-MnS 1D nanostructures.

Starting from elemental Mn and S, α-MnS nanorods (40-60 nm × 0.5-1.2 μm) were prepared by a hydrothermal route [35]. Mn metal (10 mmol) and S powder (10 mmol, Mn:S = 1:1) were suspended in water and then heated at 240–260°C for 14–20 h. XPS showed that the product composition is Mn:S = 1.1:1 and XRD gave a clean α-MnS pattern. The product observed in the SEM and TEM images had nanorod morphology (diameter 40–60 nm and length 0.5–1.2 μm) with a constant width and a high aspect ratio (13–20). The authors investigated the effect of various synthetic conditions. At temperature lower than 240°C, $Mn(OH)_2$ or impure products formed and a low yield was observed when the reaction time was shorter than 10 h. When no sulfur was used, hexagonal $Mn(OH)_2$ nanorods were obtained. The authors then proposed that α-MnS nanorods formed in a two-step mechanism where $Mn(OH)_2$ nanorods first formed which then converted to α-MnS nanorods upon the action of sulfur, a process driven by the low aqueous solubility of MnS. MnS nanorods [39] were synthesized by autoclaving for 20 h at 150°C in an aqueous solution of $MnCl_2$ and thiourea (both 1 M, Mn:S 1:1) in the presence of a through-hole anodized aluminum oxide (AAO) template previously impregnated with $MnCl_2$. The produced nanorods have homogeneous morphology (diameter 60–80 nm, length 700–800 nm) and are densely packed perpendicularly to the AAO template. It is surprising that such homogeneous morphology does not correspond to a pure crystal phase. Indeed, XRD showed the presence of both α- and γ-MnS in comparable amounts. The authors also showed that the morphology can be controlled by varying the concentration of the precursors. When the latter is increased to 2 M, arrays of MnS nanowires (diameter 60–80 nm, length 30–40 μm) are obtained while MnS nanosheets (thickness 150–190 nm, width 10–15 μm) are produced when the concentration is lowered than 0.5 M. A similar hydrothermal technique was used to prepare γ-MnS nanorods-tetrapods [14] by autoclaving an aqueous solution of Mn(II) chloride tetrahydrate (21.4 mM), Na_2S (42.8 mM, Mn:S 1:2), and ammonia (~1 M). The tetrapods have reasonably good morphology: each branch is a nanorod with a diameter of ~50 nm and a length of ~250 nm. XRD showed that they are pure γ-MnS and the growth direction along the [001] direction was determined by HRTEM. Additional experiments showed that the tetrapods formed by the self-assembly of independent nanorods. These nanosystems are promising materials for supercapacitor applications (see below).

CVD has been employed to synthesize γ-MnS 1D nanosystems with a peculiar comb-shaped morphology [10]. $MnCl_2$ and sulfur powder (Mn:S = 1:3) were used as precursors and $AuCl_3$ treated (001) silicon was used as a substrate. In this way, nanoribbons with one smooth edge and one saw-toothed edge were obtained and referred to as nanosaws. The product is mainly γ-MnS but a small amount of β-MnS was also observed by XRD. The nanosaws are over 25 μm long and 100–350 nm wide (the width is uniform all along the ribbon). The saw-teeth protrudes 10–50 nm from the (imaginary) flat baseline. Combining ED and HRTEM data, it was found out that the nanosaw long axis is parallel to the $[01\bar{1}0]$ direction and that the nanosaws have (0001) side faces and $(2\bar{1}\bar{1}0)$ top and bottom faces; the teeth direction is along [0001]. The chemical composition of the nanosaws was investigated at nanometer resolution using EELS and EDX and it turned out that the nanosaws have homogeneous composition with Mn:S close to 1:1. Further accurate HRTEM investigations showed that the thickness of the nanosaws decreases from 30-50 nm at the smooth edge to a few nanometers at the teeth and provided enough information for the authors to propose the following two-step growth mechanism. First, nanoribbons are formed

along the [01$\bar{1}$0] direction with (0001) side faces. Subsequently, the teeth grow in the [0001] direction starting from a Mn-terminated polar (0001) side face due to the polarization and termination of these crystal surfaces. The photoluminescence and potentiality as Li-ion battery electrode materials of γ-MnS nanosaws have also been investigated (see below).

2.2.2. Nanowires

A brief description of α-MnS nanowires obtained by atmospheric pressure CVD using $MnCl_2$ and sulfur powder as precursors and $AuCl_3$ treated (001) silicon as a substrate was reported in Refs. [47, 48] but unfortunately only SEM images and XRD pattern were given. A more detailed study regarding Cd-doped α-MnS nanowires synthesized by CVD was later published [49]. In this case, $MnCl_2$ and CdS were used as precursors and the Cd content was controlled by varying the temperature of the Mn source between 600 and 700°C. We here focus on the almost pure MnS nanowires that gave a clean α-MnS pattern in the XRD plot. The nanowires are about 20 μm long and have an average diameter of 70 nm. ED and HRTEM data showed that the growth direction is along [110]. The chemical composition was studied by EDX: a line scan perpendicular to the nanowires long axis gave a Mn:S ratio close to 1 and a Cd content lower than 1%. These conclusions were confirmed by XPS. The photoluminescence and magnetic properties of these α-MnS nanowires have also been investigated (see below).

To improve the performance of a supercapacitor material comprising γ-MnS nanorods-tetrapods, the same group synthesized another 1D γ-MnS nanomaterial by a hydrothermal method involving autoclaving for 2 h at 120°C an aqueous solution of Mn(II) chloride tetrahydrate (8.4 mM), thiourea (44 mM, Mn:S 1:5), and KOH (3.3 mM) [14]. They obtained a mixture of γ-MnS nanowires (diameter 10–20 nm, length 0.5–3 μm, growth direction [102]) and mixed-phase MnS NCs (10–20 nm). The authors attributed the presence of the NCs to fracture of the nanowires induced by lattice expansion due to the formation of manganese hydroxysulfide during the synthesis. This mixed product was used to fabricate an asymmetric supercapacitor (see below).

Purer samples of γ-MnS nanowires have been prepared by autoclaving for 18 h at 120°C a solution of Mn(II) acetate (1.44 mmol), thiourea (7.88 mmol, Mn:S ≅ 1:5.5), and ethylenediamine in water (pH ~10) [56]. XRD showed that the product is predominantly γ-MnS but some α-MnS is present. The product has nanowire morphology and interestingly comprises two types of nanowires. The primary nanowires occur in bundles and have a hexagonal cross section and [0001] growth direction. The second-type nanowires do not form bundles and have a rectangular cross section and [1$\bar{1}$00] growth direction. Unfortunately, quantitative size data are not provided and we can only roughly estimate the width of nanowires at 20 and 70 nm for [0001] and [1$\bar{1}$00] nanowires, respectively. When the nanowires deposited on a TEM copper grid were placed in a NaCl aqueous solution, copper from the grid substituted for manganese in the wurtzite γ-MnS lattice, but very differently for the two nanowires types. Primary γ-MnS nanowires pseudomorphically transformed into Cu_2S nanowires (no size or shape change) thanks to the similar structure of the two crystals (recall the above described $Cu_{1.94}S$/MnS dimeric heterostructure [50]) and to the nanowire growth direction. **Figure 1** shows that the γ-MnS structure has a layered structure comprising rather compact MnS planes perpendicular

to the [0001] direction which are separated by about 0.35 nm. This interlayer space is easily accessible from the exterior, thanks to the large lateral surface of the nanowires. The substitution of Mn^{2+} with two Cu^{+} ions is thus favored by the [0001] elongated morphology of the nanowires. Conversely, in the case of [1$\bar{1}$00] nanowires, the interlayer space is less accessible and ion substitution is not favored. Indeed, as nicely demonstrated by EDX and EELS imaging (ESI), the cation exchange occurred in well-defined bands several tens of nanometer wide along the nanowires axis. Heterostructured nanowires with γ-MnS/Cu_2S nanojunctions were thus synthesized.

Another 1D nanoheterostructure involving γ-MnS nanowires has been synthesized to improve the performance of 1D γ-MnS nanosystems as electrode materials for Li-ion batteries [11]. The preparation method is similar to that used by the same authors to prepare γ-MnS nanosaws [10], but the used Mn:S ratio of 1:3 and methane gas(partial flow = 5 sccm) added to the argon flow in the furnace. The products are nanowires comprising an elongated γ-MnS nanocore conformally coated with graphitic carbon and with hexagonal cross section (see **Figure 4**). The nanowires have diameter in the range of 60–100 nm and are more than 100 μm long but they easily break into shorter nanorods upon manipulation. The heterogeneous composition of the nanowires is already visible in TEM images and HRTEM confirmed the presence of both γ-MnS, as indicated by XRD data, and graphitic carbon, as indicated by Raman spectra. HRTEM also showed that the γ-MnS nanocore growth direction is [0001] and that the γ-MnS/C interface is narrower than 0.5 nm. The nanometer-resolved chemical composition of the nanowires was deduced from EDX and EELS data, which showed that the γ-MnS nanocore has Mn:S ratio close to 1:1 and diameter in the range of 20–50 nm. Extensive mechanical and electrochemical investigations of these heterostructured nanowires are reviewed below.

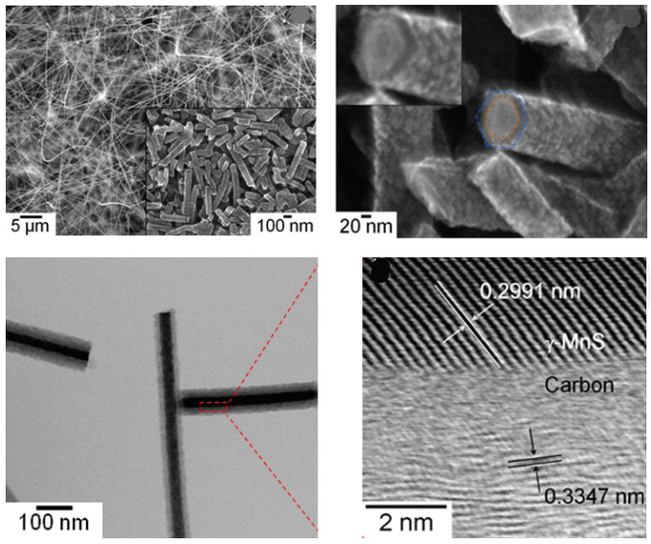

Figure 4. Electron microscopy images of γ-MnS/C nanowires. Top left:Low magnification FE-SEM image; the inset shows the nanowires after transfer onto a TEM grid. Top right: High magnification FE-SEM image showing the hexagonal cross section of the nanowires; the inset shows a close-up of an individual nanowire. TEM image (bottom left) of representative γ-MnS/C nanowires and HRTEM image (bottom right) of the γ-MnS/C interface. Adapted with permission from [11]. Copyright (2014) American Chemical Society.

2.3. Polymorphism control

In this section, we review reports where the issue of polymorphism control was purposely investigated. As early as 2001, Lu et al. [16] found that the crystal structure of the MnS sub-microcrystals, produced by autoclaving at 190–200°C a solution/suspension of $MnCl_2$ tetrahydrate and thiourea (Mn:S = 1:4), could be regulated by the solvent. In particular, γ-MnS nanorods and tetrapods were obtained using benzene as a solvent, β-MnS was prepared using THF, and α-MnS was obtained with aqueous solvents (water, aqueous ammonia, aqueous ethylenediamine). Unfortunately, the morphology of the α- and β-MnS crystallites was not given. These results were later confirmed by Ref. [38].

The formation of MnS NCs with a given crystal structure and their polymorphic interconversion could be controlled by changing thermal parameters, as expected on the basis of the different thermodynamical stability of the three polymorphs. In 2002, it was reported [17] that when MnS nanosystems were solvothermally prepared by decomposing Mn(II) di(ethyldithiocarbamate) (Mn:S = 1:4) in hexadecylamine, cubic α-MnS NCs was formed at 250°C, whereas γ-MnS nanowires and multipods with γ-MnS branches grown from a β-MnS seed were obtained at temperature lower than 150°C. The heating rate was found to affect the crystal structure of the synthetic outcome in a similar reaction where the same single precursor was dissolved in a 1:1:2 mixture of oleic acid, oleylamine and 1-octadecene and heated at 320°C [26]. By heating a reaction mixture at a rate of 15°C/min, α-MnS NCs were obtained, but larger pencil-shaped γ-MnS NCs were produced at a heating rate of 25 and 35°C/min.

The tendency toward α-MnS when the approach to equilibrium is favored was also reported in an investigation of the crystal structure of MnS sub-microcrystals obtained by injecting an aqueous solution of $MnCl_2$ in a pre-heated alkaline solution of NaHS (Mn:S ≅ 4:1) in a pressurized reactor (note the absence of organic reagents) [42]. The initial MnS polymorph formed upon mixing is dependent on the reaction temperature. α-MnS sub-microcrystals formed within 5 min after injection when the reaction temperature was higher than 325°C, whereas a pure γ-MnS product was obtained when the reaction temperature was 235°C. At room temperature, the initial product is a mixture of γ- and β-MnS NCs, which underwent crystal phase transformation upon heating. Pure γ-MnS crystallites were obtained by treating the reaction mixture at 150°C for 3 days while complete transformation into the thermodynamically stable α-MnS phase required temperature higher than 200°C for 3 days. In view of these results, the authors noted that it is unclear whether α-MnS sub-microcrystals prepared by injection at 325°C directly formed as such or precipitated as γ-MnS crystallites that quickly transformed into α-MnS within the 5-minute reaction time.

Pure samples of all three MnS polymorphs were synthesized again by changing the reaction temperature in a solvothermal protocol [40]. In this investigation, pressure-induced crystal phase transformation of MnS nanosystems was also reported. Anhydrous $MnCl_2$ (0.5 mmol) and thioacetamide (0.5 mmol, Mn:S = 1:1) were dissolved in oleylamine (5 ml) and autoclaved for 30 min at various temperatures. At 200°C, 15 nm β-MnS NCs were obtained while γ-MnS bipods with β-MnS cores were produced at 230 and 250°C. Pure γ-MnS rods (340 × 50 nm) were obtained at 270°C and large (ca. 500 nm) spherical α-MnS NCs formed at 280°C. These results show that small temperature differences strongly affect the product crystal structure.

However, the effect of pressure is the most interesting part of this report. Samples of β-MnS NCs and γ-MnS bipods (with β-MnS core) were compressed in a diamond anvil cell and their transformation into denser α-MnS was followed by XRD (see **Figure 5**). β-MnS NCs were more resistant to pressure (transformation in the range of 5-3–8.3 GPa) compared to γ-MnS bipods (2.9-4.7 GPa). The authors also showed that these transformations are first-order phase transitions with volume decrease of 18% (β-MnS NCs) and 25% (γ-MnS bipods).

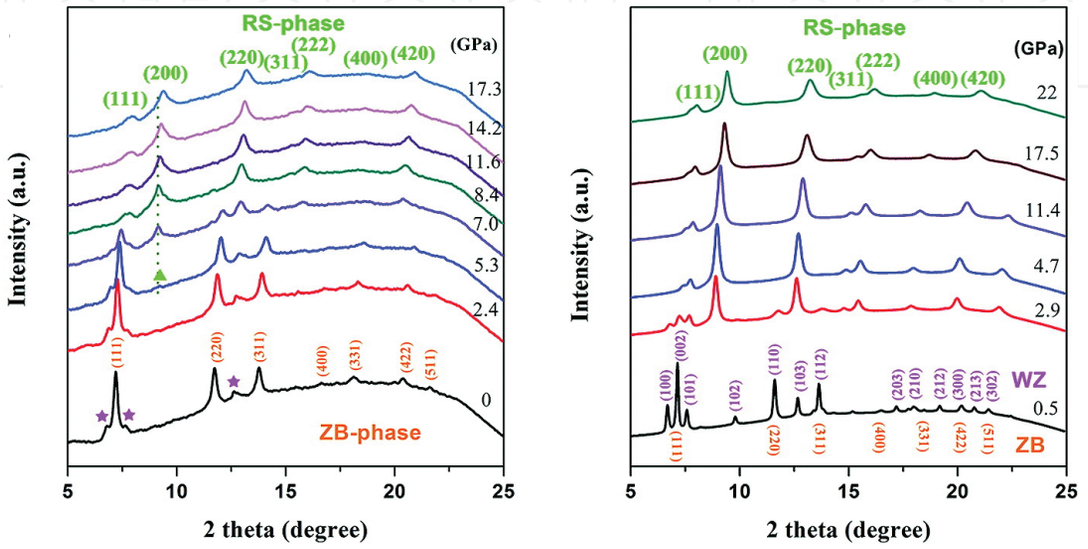

Figure 5. High-pressure XRD patterns of β-MnS NCs (left) and γ-MnS bipods with β-MnS core (right). Legend: RS = α-MnS, ZB = β-MnS, WZ = γ-MnS. The stars and triangle in the left panel represent diffraction peaks from γ-MnS and the (200) peak of α-MnS, respectively. Adapted with permission from [40]. Copyright (2012) American Chemical Society.

In addition to the variation of physical parameters, control of the polymorphism of MnS nanosystems can also be achieved by chemical means. In Ref. [34], it was briefly mentioned that using a higher (lower) sulfur content in a solvothermal protocol involving heating at 200°C a solution of Mn(II) nitrate and sulfur powder in octadecylamine produces large α-MnS NCs (micrometer-size γ-MnS nanorods) but no detail was reported. The importance of both physical and chemical parameters in polymorphism control was ascertained for a solvothermal reaction involving autoclaving a solution of $MnCl_2$ (3.2 mmol), sulfur powder (3.0 mmol, Mn:S = 1:0.94), and KBH_4 (5.0 mmol) as a reducing agent in ethylene glycol. At low temperature (≤180°C), hollow 300–500 nm spherical aggregates composed of 30–40 nm γ-MnS NCs formed, as determined by SEM, TEM, and XRD, with composition Mn:S = 1:1.03 from ICP data. These are the optimum conditions for the preparation of γ-MnS, any change in reaction conditions induced the partial or complete formation of α-MnS. This of course includes an increase in temperature but also the solvent as ethanolamine and ethylenediamine yielded α-MnS. The role of the reducing agent is also interesting. KBH_4 is necessary to prepare γ-MnS but the stronger reductant hydrazine produced α-MnS. In general, it seems that the presence of amino groups, either in the solvent molecule or in the reductant, favors the formation of α-MnS. Similar results were obtained for the hydrothermal reaction [51] of $MnCl_2$ tetrahydrate (1 mmol) with Na_2S nonahydrate (1.5 mmol, Mn:S = 1:3) at 180°C for 9 h yielding γ-MnS sub-

http://dx.doi.org/10.5772/65092

microrods (diameter 200–300 nm, length 1–1.5 μm) with a hexagonal cross section. However, when 34 mmol of hydrazine was added to the reaction mixture, α-MnS octahedral submicrocrystals (edge length 170–200 nm) were formed. It was ascertained that neither pH nor temperature (120°C–180°C) affects the synthetic outcome. However, carrying out experiments with different reaction times and observing that treatment of the γ-MnS nanorods with hydrazine gave α-MnS led the authors to propose that α-MnS crystallites originated from redissolution of γ-MnS nanorods mediated by the formation of a hydrazine-manganese complex.

Finally, an extensive study [31] on the effect of the surfactant on the crystal phase of the MnS NCs resulting from a solvothermal protocol was carried out. The amount of sulfur needed to obtain MnS NCs by a solvothermal synthesis depends on the amount of surfactant present. A particular reaction was investigated where a mixture of (Mn precursor):sulfur:surfactant 2:4:1 dissolved in 1-octadecene was heated to 320°C (heating rate = 10°C/min). As a Mn precursor, Mn distearate and $Mn_2(CO)_{10}$ were used and a wide range of surfactants were investigated, that is, stearic acid, oleic acid, hexadecylamine, dodecylamine, octadecylamine, oleylamine, oleylalcohol, and dodecanethiol. It was concluded that to prepare γ-MnS NCs from a solution of elemental sulfur and a manganese precursor in 1-octadecene, it is necessary that the reaction mixture comprises both amine and carboxylic acid surfactants, otherwise α-MnS NCs are formed. Furthermore, whether the carboxylic acid is present as a free surfactant or as a carboxylate ligand within the Mn precursor is irrelevant to the crystal structure of the resulting NCs.

3. Optical properties

Because of the growing interest in optical and optoelectronic applications, several studies reported on the optical absorption and photoluminescence (PL) spectra of MnS nanosystems, which can be useful as light emitting and optoelectronic devices in the ultraviolet spectral region [52], thanks to the wide bandgap of MnS and blue-shifting quantum confinement effects.

The optical absorption spectra of 0D α-MnS NCs were described in several reports. Hydrothermally synthesized 30-nm spherical α-MnS NCs displayed a well-defined absorption band peaking at 261 nm (4.75 eV) [38]. Larger NCs showed broader absorption peaks. Star-shaped ~100-nm hexapods exhibited a broad peak at ca. 360 nm (3.4 eV) and ~200-nm hexagonal NCs had a similar peak but red-shifted to ca. 370 nm (3.3 eV) whereas the absorption spectrum of intermediate-size octahedral NCs is almost featureless [26]. Size-dependence of the absorption spectrum was observed for ordered aggregates of α-MnS nanocubes with edges 14, 26, and 40 nm [52]. The spectra are almost featureless but peaks in the near ultraviolet (337, 346, and 355 nm for 14, 26, and 40 nm nanocubes, respectively) were discerned and attributed to the transition to the excitonic state. The blue-shift from the 388 nm transition of the bulk material is sizeable and modulated via the nanocubes edge length.

Photoluminescence of 0D α-MnS NCs was only reported in the case of size-controlled nanocubes, [52], which when excited at 300 nm emit in the near ultraviolet range at room temperature. The PL maximum is size dependent and ranges from 356 to 373 nm (3.48–3.23 eV) when the cube edge grows from 14 to 40 nm, showing the effects of quantum confinement. This phenomenon and the NC size control afforded by wet nanocrystal chemistry techniques make size-controlled α-MnS NCs promising materials for emitting devices in the ultraviolet region. PL was also investigated in 1D α-MnS NCs. Hydrothermally synthesized α-MnS nanorods (40–60 nm × 0.5–1.2 μm) excited at 273 nm at room temperature displayed a strong, narrow PL peak at 400 nm (3.1 eV), corresponding to the good size dispersion and crystal quality of the nanorods [35]. A more in-depth investigation of the PL of α-MnS nanowires (pure and Cd^{2+}-doped) was later reported in Ref. [49]. We here focus on the pure α-MnS nanowires that are about 70 nm in diameter and grown along the [110] direction up to about 20 μm in length. Their PL was observed after excitation at 325 nm between 7 and 300 K and comprised two bands. The broad and weak band at ca. 2.9 eV (428 nm) was attributed to band-edge emission involving the excited states of the Mn^{2+} ions. The other band centered about 1.6 eV (775 nm) has strongly temperature-dependent intensity and vanishes at temperature above ~150 K (see **Figure 6**). This band was attributed to the decay of impurity-perturbed Mn^{2+} excited states. Time-resolved PL of the 1.6 eV band after excitation at 266 nm showed that its average decay time at 7 K is 40 μs.

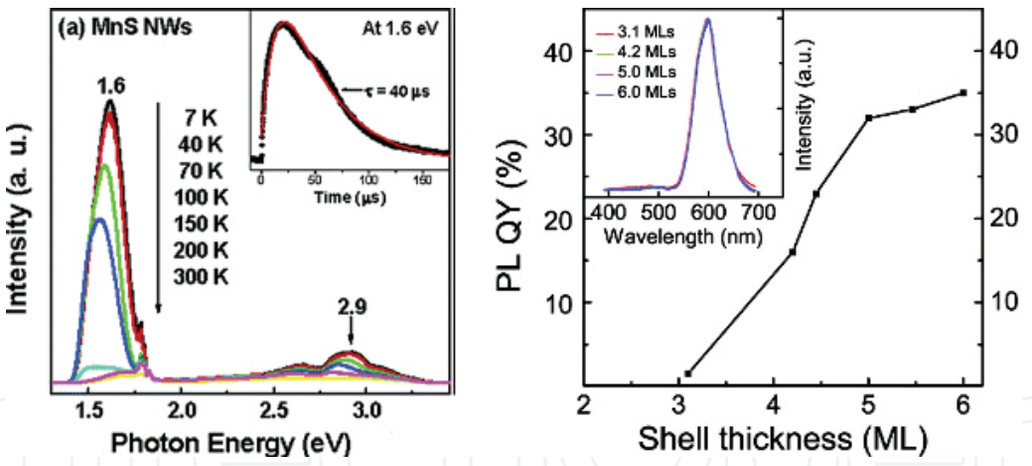

Figure 6. Photoluminescence of MnS nanosystems. Left: Temperature dependence of the photoluminescence spectrum of α-MnS nanowires measured between 7 and 300 K after excitation at 325 nm; the time resolved photoluminescence of the 1.6 eV band after excitation at 266 nm (4.66 eV) is shown in the inset. Adapted with permission from [49]. Copyright (2006) American Chemical Society. Right: Photoluminescence quantum yield of β-MnS@ZnS core–shell nanoparticles as a function of the ZnS shell thickness (1 ML = 0.31 nm); the normalized photoluminescence spectra at room temperature are shown in the inset. Reprinted with permission from [45]. Copyright (2009) American Chemical Society.

The PL of β-MnS nanosystems received some attention. The photoluminescence excitation (PLE) spectra, obtained by monitoring the intensity of the PL while varying the excitation wavelength, showed several well-resolved peaks attributed to the transition from the ground $^6A_1$ state to the excited states of Mn^{2+} ions. Interestingly, the $^6A_1 \rightarrow {}^4T_2(4D)$ transition undergoes

a shift at temperatures below the Néel temperature of the bulk material revealing the strong correlation between the energy of the Mn-internal optical transitions and the magnetic transition from the paramagnetic state to the antiferromagnetic state. The optical properties of β-MnS@ZnS core-shell nanoparticles were studied in detail in Ref. [45]. By a two-step one-pot solvothermal procedure, β-MnS@ZnS core-shell heterostructures were synthesized with equally-sized β-MnS NC cores (diameter 2.3 nm) and the ZnS shell of varying thickness (0.9–1.8 nm). The PL spectrum (excitation at 325 nm) comprises the "orange" peak at ca. 600 nm (2.1 eV), the position of which is almost independent of temperature and shell thickness. The PL quantum yield instead grows rapidly with ZnS thickness, from 1.5% for the 0.9 nm thick shell to 35% for the thickest shell (see **Figure 6**). The authors showed that a large increase in PL quantum yield is mainly due to the enhancement of the energy transfer from the ZnS shell to the core Mn^{2+} ions, though a small contribution from a slight decrease in non-radiative relaxation from Mn^{2+} ions to surface states/traps brought about by the thicker ZnS shell cannot be excluded. Interestingly, while the PL quantum yield has a strong dependence on the ZnS shell thickness, the PL lifetimes at room temperature are rather insensitive to the shell thickness. In a second report [46], the same group studied the relationship between PL and the diffusion of Mn^{2+} ions into the ZnS shell occurring when a final annealing step was added to the synthetic protocol. Annealing had a detrimental effect on the PL quantum yield, which was attributed to the diffusion of Mn^{2+} ions into the ZnS shell that causes an increase in non-radiative relaxation, as also evidenced by the significant decrease of the PL lifetime upon annealing. It was shown that Mn^{2+} ions can diffuse into the shell at temperatures as low as 220°C.

Based on this concept, another group prepared small (5.5–6.5 nm) 0D ZnS@MnS@ZnS heterostructures by a hydroalcoholic co-precipitation protocol [6]. These triple-layer nanoparticles display a narrow intense "orange" PL band in addition to the short wavelength peaks attributed to defects in the ZnS lattice. The wavelength of the "orange" peak gradually shifts from 742 to 750 nm upon increasing the amount of Mn precursors in the synthesis, which presumably corresponds to increasing thickness of the MnS layer. The authors propose several explanations for the systematic red shift upon increasing the Mn content. This effect could be due to size-dependent electron-phonon coupling and crystal-field effects but they can also be related to the incorporation of Mn^{2+} ions into the ZnS lattice. Finally, long β-MnS nanowires (diameter ca. 25 nm) have a clearly defined absorption band at 371 nm (3.34 eV), described as an excitonic transition, and a Gaussian-shaped PL peak at 488 nm (2.54 eV), the shape of which was interpreted by the authors as evidence of the good monodispersion and surface passivation of these solvothermally prepared nanowires [27].

We are aware of a single report on the optical properties of 0D γ-MnS NCs, whereas 1D γ-MnS nanosystems have attracted some attention. Small (3–11 nm) γ-MnS NCs grown inside mesoporous silica exhibited the so-called "orange" band at 2.1 eV (590 nm) when excited at 325 nm [43]. Thin γ-MnS nanowires (diameter 2.2 nm, aspect ratio ~80) displayed an absorption band edge at 3.64 eV (341 nm) and a well-defined PL peak centered at 3.34 eV (371 nm), which therefore seem to be promising as near ultraviolet emitters [17]. A morphologically heterogeneous sample of γ-MnS rod-like and branched nanosystems (with an aspect

ratio of 6–10) displayed a very broad absorption band at 278 nm (4.46 eV) and very weak PL with peaks at 368 and 438 nm (3.37 and 2.83 eV), both attributed to band edge emission (no trap state emission was detected) [38]. The optical properties of CVD-synthesized γ-MnS nanosaws (length ~25 μm in the [01$\bar{1}$0] direction, width = 100-350 nm) were analyzed in detail in Ref. [10]. The PL spectrum of the nanosaws was recorded at temperature between 10 and 300 K after excitation at 325 nm. Three PL bands were described. Two relatively weak bands were ascribed to (blue-shifted) exciton-related band edge emission (371 nm, 3.34 eV) and surface defect emission (430 nm, 2.88 eV). The predominant band is the "orange" band at 582 nm (2.13 eV), which is attributed to the radiative recombination of electrons in surface state shallow traps with photogenerated holes caused by lattice stacking faults. The "orange" band is 10^4 times more intense than the exciton-related band, which is in agreement with the high density of stacking faults evidenced by HRTEM. The PL intensity of the "orange" band decreased quickly when the temperature was below 100 K, to be compared with the Néel temperature of bulk γ-MnS (~80 K). Indeed, the antiferromagnetic ordering of the Mn^{2+} ions contributes to the carrier transfer of electrons from the conduction band to donor states. By fitting the thermally activated carrier transfer model to the temperature dependence of the "orange" band intensity, it was determined that the donor states are ~40 meV below the conduction band. This result supports the claim that the donor states are associated with surface states. The lifetime of the "orange" band at 300 K turned out to be 44 μs, shorter that the bulk value (140 μs) further supporting the view that the high surface/volume ratio of the nanosaws facilitates energy transfer from Mn^{2+} excited states to surface states and thus accelerates non-radiative relaxation.

In summary, all α-MnS NCs show band-edge emission but only 14–40 nm nanocubes are able to emit in the ultraviolet range. The "orange" band was only observed in the spectrum of the thicker and longer α-MnS nanorods. Small (2–11 nm) 0D β-MnS NCs, both uncoated and ZnS-coated, display the "orange" peak at 2.1 eV in the PL spectrum, while β-MnS nanowires (diameter 25 nm) have a significantly blue-shifted PL peak at 2.54 eV; ZnS-coated β-MnS NCs have an attractive PL quantum yield of 35%. Very thin γ-MnS nanowires emit in the near ultraviolet, whereas large nanosaws are good "orange" emitters. In conclusion, the optical properties of MnS nanostructures are very sensitive to morphology and crystal defects so that tight synthetic control is required to obtain good performance. Interesting results, especially in the near ultraviolet region, have been demonstrated, and MnS remains a promising candidate as an emitter in the range 340–380 nm.

4. Electrical properties and applications

Recently, electrical properties and applications of MnS nanosystems have attracted much interest. Indeed, several studies showed that MnS NCs are promising materials as electrodes for lithium ion batteries (LIBs) [10–13, 53] and as supercapacitors [14, 15]. However, the first electrical characterization in 2008 was the measurement of the current-voltage (*I-V*) curve of α-MnS nanobelts [37] obtained by an autoclave solvothermal technique. The nanobelts grow along the [100] direction and are longer than 1 μm, 50–150 nm wide and 25 nm thick. Several

measurements of single nanobelts gave a linear *I-V* response between −1 and +1 V (ohmic behavior) with a specific conductance of 3.4×10^5 S/m, comparable to that of 1D ZnO or In_2O_3 nanosystems grown by physical methods.

The use of crystalline nanomaterials to build electrodes for LIBs has gathered much attention since nanomaterials have a high surface/volume ratio, reduce Li diffusion length, are able to accommodate crystal strain, can be processed from solution, and can be produced by the rich toolbox of colloidal chemistry, which enables one to control the nanomaterial composition, size, and shape. It is noteworthy that all three MnS polymorphs have been investigated as nanosized LIB electrode materials. To put the capacity values reported below in the appropriate framework, we recall that the theoretical capacity of MnS is 616 mAh g^{-1}. Sub-micrometric α-MnS crystals, hydrothermally-grown at different temperatures, were mixed with carbon black and a polymeric binder (8:1:1 w/w) and spread on copper foil. These electrodes showed good performance [53]. All samples exhibited a lithiation plateau at about 0.7 V versus Li/Li^+, which corresponds to the Li^+ insertion in MnS and evidences that the α-MnS sub-microcrystals are suitable anode materials for LIBs. The α-MnS sample prepared at the lowest temperature (120°C) displayed the highest initial lithiation capacity (1327 mAh g^{-1}), thanks to the small particle size (150–600 nm). In all cases, however, the lithiation capacity is sharply reduced in the second cycle and then it decreased slowly upon cycling. The large irreversible decrease between the first and second cycles was attributed to the formation of a solid electrolyte interface film on the surface of the electrode. Considering the overall behavior, the best electrode is prepared using particles synthesized at 160°C (about 700 nm in size) which maintained a capacity of 578 mAh g^{-1}, corresponding to ca. 81% of the second lithiation capacity, after 20 cycles. The authors attributed this performance to the better crystallinity of the 160°C α-MnS sub-microcrystals.

Recently, β-MnS NCs were used to prepare promising electrode materials for LIBs without employing any binder or conductive filler (e.g., carbon black) [13]. The solvothermally prepared ~15 nm β-MnS NCs were first electrophoretically deposited on copper plates and then stripped of their organic ligand coating by either heating at 300°C or dipping in a methanolic solution of ammonium sulfide. The charge-discharge curves and the capacity retention on cycling of both heat-treated and dipped β-MnS NC film electrodes are shown in **Figure 7**. These electrodes showed a lithiation plateau at 1.7 V, stable for more than 50 cycles, which makes them suitable as cathodes in LIBs. The electrodes showed excellent stability with a final capacity of 420 (dipped) and 470 mAh g^{-1} (heated) after more than 50 charge-discharge cycles. The good performance of these electrodes was attributed to the improved interparticle coupling and electrical properties (e.g., electrical conductivity) obtained by the combination of electrophoretic deposition and ligand stripping which allowed the authors to prepare electrodes free of additives and organic ligands.

Finally, also 1D γ-MnS nanosystems were used as electrodes due to their potential application for LIBs. CVD synthesized γ-MnS nanosaws (length ~25 μm in the $[01\bar{1}0]$ direction, width = 100–350 nm) were mixed with carbon black and a polymeric binder (7:2:1 w/w) and spread on copper foil [10]. This electrode showed good performance in the initial cycle with a capacity of 1150 mAh g^{-1} and an extended plateau at ~0.5 V. The performance,

however, degraded rapidly with cycling (second cycle capacity = 780 mAh g^{-1}, after 40 cycles capacity ~200 mAh g^{-1}) and the voltage plateau disappeared. To improve the electrochemical performance, the authors succeeded in synthesizing γ-MnS nanowires (aspect ratio ≈1000) conformally coated with graphitic carbon by a single-step CVD technique. The nanowires have a hexagonal section [60–100 nm, inner (γ-MnS) diameter is 20–50 nm] and are over 100 μm long in the [0001] direction. The electrodes were prepared by mixing the carbon-coated nanosaws with a polymeric binder (92:8 w/w) and spreading the mixture on a copper foil. The charge-discharge curves displayed no voltage plateau. The initial capacity of 1036 mAh g^{-1}decreased to 747 mAh g^{-1} at the second cycle and reached a good 503 mAh g^{-1} after 25 cycles. The improved results were ascribed to the presence of a highly conducting carbon layer, which is thin enough to allow Li^+ to reach the inner γ-MnS core, prevents the decomposition of polysulfides, and provides more active regions for the electrochemical reaction.

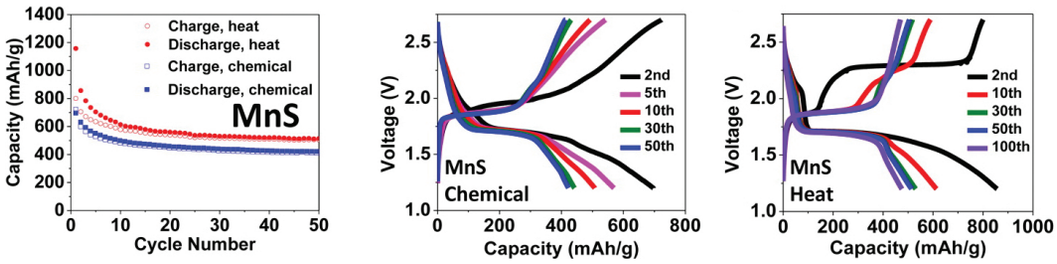

Figure 7. Electrochemical performance of β-MnS NC film electrodes without a conductive filler and a polymeric binder. Left: Capacity retention on cycling. Charge-discharge curves of chemical- (middle) and heat-treated (right) β-MnS NC film electrodes; the plateau at 1.7 V can be clearly seen. Adapted with permission from [13]. Copyright (2012) American Chemical Society.

Nanosized γ-MnS has very recently turned out to have exciting properties for supercapacitor applications. A supercapacitor is a high-capacity electric capacitor showing performance between conventional electrolytic capacitors and rechargeable batteries. They typically store 10–20% of the energy that one can put into a battery but supercapacitors store and release energy much faster than a battery and can withstand many more cycles because they do not rely on electrochemical reactions to charge-discharge. Supercapacitors have advantages in applications where a large amount of power is needed for a relatively short time and when a very high number of charge-discharge cycles or a longer lifetime is required. A typical application is power supply stabilization in consumer electronics: supercapacitor-powered devices (e.g. portable speakers, screwdrivers) have already reached the market. Supercapacitors are widely used to reduce energy consumption in transportation, e.g., recovery of braking energy since they can quickly store and release energy over long times with a high cycle rate.

Hydrothermally synthesized γ-MnS tetrapods (with 50 × 250 nm branches) were mixed with acetylene black and a fluorinated polymeric binder (70:15:15 w/w) and used to coat a nickel foam current collector [14]. Cyclic voltammetry showed that these electrodes have high specific capacitance even at a high rate, e.g., of 705 F g^{-1} at a scan rate of 1 mV/s and 323 F g^{-1} at 100 mV/s. This excellent performance was attributed to the intercalation of

hydroxyl ions between the MnS layers parallel to the basal crystal plane, which are easily accessible from the exterior since they are perpendicular to the nanorod axis along the [001] direction. The charge-discharge curves maintain their quasi-triangular shape at a current density as high as 10 A g^{-1}. The γ-MnS tetrapod capacitors had very good cycling performance with a capacity retention of 80% after 1000 cycles and 63% after 5000 cycles, with high and constant coulombic efficiency. The XRD investigation of cycled electrodes indicated that the performance degradation can be attributed to the transformation of the NCs from the γ- to the stable α-crystal structure. Asymmetric capacitors prepared by coupling a γ-MnS tetrapod positive electrode with a negative activated carbon electrode were shown to be purely capacitive and maintain the high rate capacity of the symmetric capacitor. The specific capacity is of course lower (59.8 F g^{-1} at 1 mV/s scan rate and 37.6 F g^{-1} at 100 mV/s) but the achieved energy density (11.7 Wh kg^{-1} at the power density of 4.45 kW kg^{-1}) is higher than that of carbon-based symmetric capacitors in aqueous electrolytes. In order to achieve better performance by improving the carbon-based-electrode, the same group later reported on an asymmetric supercapacitor comprising inhomogeneous MnS nanomaterials (NCs and nanowires, all three polymorphs present) as a positive electrode and highly porous amorphous carbon derived from eggplants [15]. These capacitors (with almost purely capacitive behavior) exhibited high specific capacitance (around 100 mAh g^{-1}) even at a rate of 100 mV s^{-1} and at current as high as 50 mA and retained 90% of the capacitance after 5000 cycles. The authors attributed this stability to the ionic accessibility and stability of the layered crystal structure of γ-MnS and showed that after being fully charged, two capacitors in series can light up a red LED indicator for 15 minutes.

5. Magnetic properties and applications

As anticipated, all three MnS polymorphs have antiferromagnetic (AFM) structure at low temperature, since the high-spins d^5 Mn^{2+} (S = 5/2) ions are antiferromagnetically coupled by superexchange interaction. The ordering (Neél) temperature T_N of bulk samples is highest for α-MnS (154 K), followed by β-MnS (~100 K) and γ-MnS (~80 K) [2]. Above T_N, all three forms of MnS are paramagnetic (PM) and follow the Curie-Weiss law $\chi = N(p_{eff}\mu_B)^2/[3k(T-\Theta)]$ with Θ = −465, −982, and −932 K for the α, β, and γ structures, respectively [19]. The effective magnetic moment corresponds to five unpaired electrons, e.g., p_{eff}= 4.54 for α-MnS [54]. The magnetic properties of MnS nanosystems have been investigated by recording the isothermal magnetization $M(H)$, useful to observe the low-temperature hysteresis loop and to measure the Curie-Weiss temperature Θ in the paramagnetic phase, and the thermal dependence of the zero-field-cooled (ZFC) and field-cooled (FC) magnetization $M(T)$, which provide information about the AFM/FM transition.

Several reports focused on α-MnS 0D NCs prepared by solvothermal techniques. Puglisi et al. [32] studied octahedral α-MnS NCs with size 14, 20, and 29 nm. The general behavior of the NCs corresponds to that observed for AFM materials. The high-temperature magnetization obeys the Curie-Weiss law with size-dependent Θ = −149 K (14 nm), −227 K (20 nm), −272 K (29 nm), much higher than the bulk value. The effective magnetic moment is close to the bulk

value, ranging from 4.6 to 4.9 μ_B. These results clearly indicate that the strength of the exchange interaction supporting the AFM order is strongly size-dependent whereas the local electronic structure of the Mn^{2+} ions is similar to that in the bulk. The low-temperature magnetization does not show cusps related to the AFM/PM phase transition but suggests the presence of some ferromagnetic (FM) materials, in particular for the 29 nm NCs which display a maximum in the ZFC magnetization at 25 K. This was confirmed by the isothermal magnetization at 5 K displaying an open loop with strongly size-dependent coercivity H_c = 9 Oe (14 nm), 81 Oe (20 nm), 180 Oe (29 nm). To ascertain whether this is due to an FM impurity or to an FM region in the NC, field-cooled hysteresis loops were recorded (see **Figure 8**). These were shifted in the direction opposite to the field by a size-dependent amount H_{shift} = 0 Oe (14 nm), −17 Oe (20 nm), −44 Oe (29 nm). This exchange bias effect is the hallmark of an exchange interaction across a FM/AFM interface and is evidence of the presence of a FM region in the NCs. In accordance with the interpretation of a similar behavior observed in several magnetic NC types, it was proposed that α-MnS displays a magnetic core-shell structure, where the outer shell of the NC is (at least partially) FM because of the under-coordination of the Mn^{2+} ions and lattice distortion near the NC surface. The FM shell is exchange coupled to the AFM core and gives rise to the open and shifted hysteresis loops observed.

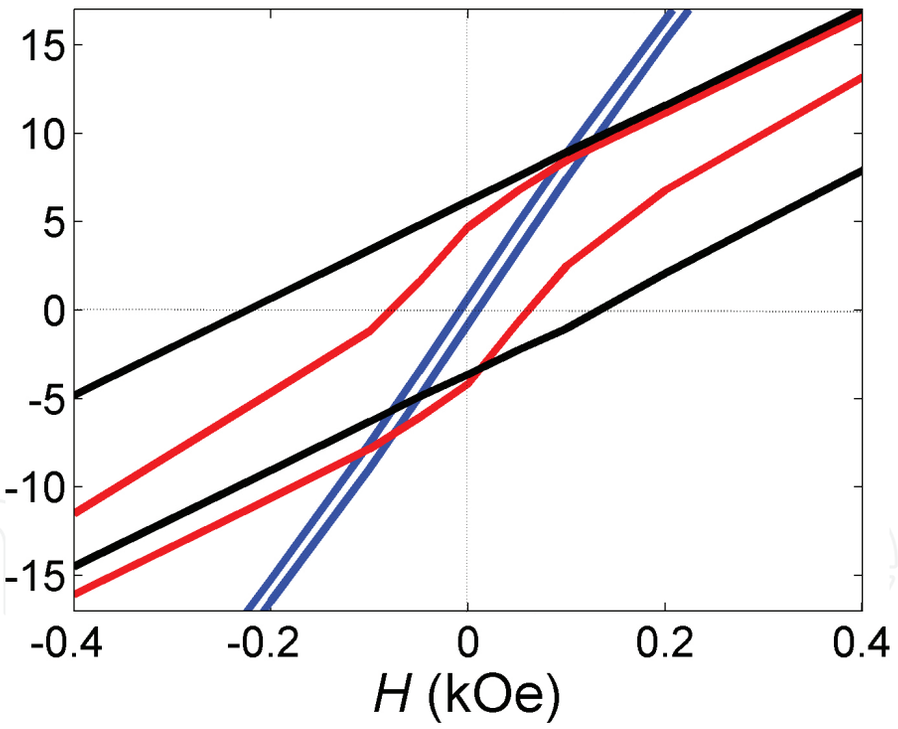

Figure 8. Low field part of the field-cooled isothermal magnetization (hysteresis loop) of 14 nm (blue), 20 nm (red), and 29 nm (black) α-MnS NC. Both the open loop and the loop shift are clearly seen.

Size-dependent magnetic properties were also measured for α-MnS cubic NCs with an edge size of 14, 26, and 40 nm [52] and further supported the core-shell model. The ZFC/FC magnetization is similar to that observed for octahedral NCs, showing at 32 K a maximum of the ZFC magnetization of 26 and 40 nm NCs. The largest NCs also reveal an increase of the FC

http://dx.doi.org/10.5772/65092

magnetization below 28 K related to the freezing of the surface spins. The low-temperature hysteresis loops confirmed the presence of an FM region since they display open loops with size-dependent coercivity ranging from 10 Oe (14 nm) to 1265 Oe (40 nm), which is in good agreement with the coercivity of octahedral NCs. The study of the magnetic properties of 45 nm star-shaped α-MnS NCs [33] again confirmed this model by showing that at 5 K the NCs have an open hysteresis loop with large H_c = 1573 Oe; the authors pointed out that the FC magnetization increase below 150 K is related to the freezing of the surface spins in an FM-like shell. In their pioneering article, Kan et al. [18] also studied the magnetic properties of spherical α-MnS NCs with size 20, 40, and 80 nm. They found a generally AFM behavior with size-dependent T_N (50, 97, and 116 K) and Θ (−59, −86, and −174 K) for 20, 40, and 80 nm NCs, respectively. Again, this indicates that the AFM magnetic ordering is less effective at small size. These Θ values are, however, high when compared to the size trend displayed by octahedral NCs [32], and their hysteresis loop is closed. This suggests that these spherical NCs actually are agglomerates of smaller NCs, a conclusion also supported by the TEM images.

Two facts about the magnetic properties of 0D α-MnS NCs are generally agreed upon. First, the NC core undergoes a low-temperature AFM transition characterized by negative Curie-Weiss temperature Θ that approaches the bulk value (−465 K) as the NC size increases. Second, the NC surface spins form an FM-like layer, which is clearly observed in the low-temperature hysteresis loops. The observed coercivity ranges from the hundreds of Oe for 20–30 nm octahedral NCs to the kOe range for 40 nm nanocubes and 45 nm nanostars. Exchange coupling between the AFM core and the FM shell has been detected as a shift (exchange bias) of the field-cooled hysteresis of octahedral α-MnS NCs [32].

The magnetic properties of 1D α-MnS nanosystems have also been studied. α-MnS nanowires, slightly doped with Cd, have been grown by CVD to about 20 μm length and average diameter 70 nm [49]. The growth direction is along [110]. They generally behave as an AFM material both at low temperature (where they display closed isothermal magnetization curves) and at high temperature (T > 100 K) where they follow the Curie-Weiss law with Θ = −903 K. This value is much higher than the bulk value, suggesting a remarkably stronger AFM correlation in the nanowires than in the bulk. The authors hypothesized that the stronger AFM could be caused by the intrinsic geometrical anisotropy of the nanowires but did not exclude that the Cd^{2+} impurity played a role. We also remark the absence of magnetic signatures indicating the presence of an FM-like phase at the nanowires surface. The magnetism of α-MnS nanobelts has also been characterized [37]. These nanobelts, obtained by an autoclave solvothermal technique and grown along the [100] direction, are longer than 1 μm, 50-150 nm wide and 25 nm thick. An FM-like shell since was present since the hysteresis loop at 5 K is open with coercivity H_c = 4013 Oe, a large value that might be due to the relatively high surface/volume ratio of the nanobelts with respect to the 0D NCs. It remains unclear why these nanobelts have an FM-like shell while the above nanowires do not. We can tentatively propose that the reason is that the nanowires prepared by CVD are free from organic coating on the surface (the nanobelts are stabilized by dodecylamine) and perhaps have a better lattice quality in the near-surface region.

The magnetic properties of γ-MnS nanosystems have been rarely reported. However, a detailed study of 0D γ-MnS NCs has been described. Spherical γ-MnS NCs with size 3–11 nm were prepared by intrapore synthesis inside mesoporous silica [43]. The high-temperature part of the NC magnetization versus temperature curve follows the Curie-Weiss law with Θ ranging from about −500 K (11 nm) to about −100 K (6 nm). It is noteworthy that 3 nm γ-MnS NCs closely follow the Curie-Weiss law down to 2 K, indicating that AFM ordering is not present even at such low temperature. Therefore, the behavior of γ-MnS NCs agrees with the conclusion drawn for α-MnS NCs, i.e., the onset of AFM ordering occurs at lower temperature for smaller NCs. Deeper insight into the magnetism of the γ-MnS NCs was obtained by studying their electron paramagnetic resonance (EPR) spectrum. EPR is a local probe of the magnetic state of transition ions but, because of the strong interactions between Mn^{2+} ions, the EPR spectrum appears as a broad line without any resolved feature from zero-field or hyperfine interaction. Careful analysis of the temperature-dependent EPR spectra showed that they are actually composed of a broad and a narrow line, the latter following the purely PM Curie law. The broad line follows the Curie-Weiss law with negative Θ typical of AFM materials and the EPR-derived Θ values closely agree with those derived from magnetization measurements, evidencing that the broad EPR line corresponds to the AFM ordered core of the NCs. Since optical measurements showed that the Mn^{2+} exchange constant does not depend on size, the strong decrease in the AFM onset with size was attributed to the presence of a disordered PM shell. By analyzing the relative intensity of the broad (AFM) and narrow (PM) EPR lines, the authors could conclude that the surface/volume ratio is critical to determine the onset of the long-range ordered AFM phase and that the minimum diameter to observe AFM ordering of γ-MnS NCs at non-zero temperature is between 3 and 6 nm, corresponding to 1000–4000 Mn^{2+} ions.

Heterostructures consisting of a 16 × 16 nm γ-MnS nanocylinder epitaxially grown on a 16 × 4 nm $Cu_{1.94}S$ nanoplate were synthesized by a solvothermal technique [50]. The isothermal magnetization curve is purely PM but no conclusion can be drawn since the measurement temperature is not specified. The magnetic properties of solvothermally prepared γ-MnS nanorods (2.4 × 20 nm) were measured [17]. The isothermal magnetization at 5 K displayed an open loop with large coercivity (H_c = 1020 Oe) and the ZFC magnetization showed a maximum at 30 K. These observations support the presence of an FM-like shell surrounding an AFM core, as occurs in α-MnS nanosystems. The large coercivity is expected on the basis of the large surface/volume ratio of 1D nanosystems.

No magnetic characterization of β-MnS NCs seems to have been reported except for a brief EPR study. The RT EPR spectrum of solvothermally prepared β-MnS nanowires with 25 nm diameter was described [27] as a single line at g = 2.0064 with linewidth about 1000 Oe, typical of strongly coupled high-spin Mn^{2+} ions. The line shape is asymmetric reflecting the morphological anisotropy and inhomogeneity of the sample. The linewidth is larger than that observed for 0D γ-MnS NCs (about 500 Oe for 11 nm NCs) [43] as expected on the basis of the nanowire diameter. Finally, a mixture of α-, β-, and γ-MnS NCs (size 3.5–5.1 nm) within the 7 nm pores of mesoporous P123 silica displayed ZFC/FC curves similar to those observed for α-MnS NCs, with a maximum at T = 42 K attributed to the FM-like surface shell of the NCs. The presence

of such an FM-like region was confirmed by recording isothermal hysteresis loops between 10 and 50 K. The loops up to 35 K are open and support the presence of an FM-like component while the loop at 50 K is purely reversible. Coercivity values were not given.

In conclusion, the magnetic properties of MnS nanosystems can mostly be understood on the basis of the magnetic core-shell model where just the nanosystem core undergoes a size-dependent AFM transition (the smallest the size, the lowest the transition temperature) whereas the nanosystem surface shell form a FM-like (α- and γ-MnS) or PM (γ-MnS) layer. We recall that the observation of exchange bias shifted hysteresis loops in octahedral α-MnS NCs [32] is a strong evidence of the presence of an FM/AFM interface.

As a very promising application of the magnetism of MnS, we mention a report demonstrating very good performance of α-MnS NCs as a T_1 contrast agent for MRI [9]. The usefulness of α-MnS microparticles as a T_1 contrast agent had been demonstrated as early as 1985 [8] and very recently, α-MnS NCs were shown to have larger T_1 relaxivity than a commercial gadolinium-based contrast agent. Solvothermally prepared (5 ± 2) nm α-MnS NCs were coated with citrate to obtain a stable NC dispersion in water. It was shown that they have T_1 relaxivity = 3.4 mM^{-1} s^{-1} in water and 8.7 mM^{-1} s^{-1} when bovine serum albumin (BSA) was added to the aqueous dispersion to simulate the protein content of blood. These NCs have larger T_1 relaxivity than most reported values for the widely studied Mn oxide (MnO and Mn_3O_4) NCs and, more importantly, than the commercial T_1 contrast agent Gd-(diethylenetriaminepentacetic acid) complex. This means that 5 nm α-MnS NCs can provide equal image contrast with a ca. tenfold lower dose. In vitro viability assays showed that these NCs are not cytotoxic to HepG2 cells up to a dose of 70 μg/ml. In vivo T_1-weighted images of a nude mouse at 0.47 T showed good contrast in liver and kidneys 1 h after injection. Thus, α-MnS NCs undergo the usual fate of IV injected NCs, that is capture by the liver MPS cells. Thanks to their very small size, the NCs are partially excreted through the renal pathway. The uptake and excretion rate, both for liver and kidneys, are similar to that of the commercial Gd-based T_1 agent.

6. Other

The mechanical properties of individual heterogeneous γ-MnS@(graphitic carbon) nanowires synthesized by CVD have been measured using an AFM holder in a TEM chamber [11]. The nanowires have hexagonal section (60–100 nm) and are over 100 μm long in the [0001] direction; the inner γ-MnS core has a diameter of 20–50 nm. Under uniaxial compression, the nanowires first underwent a weak plastic deformation followed by fracture in brittle mode at a critical force of 1330 nN. The fracture occurs perpendicular to the nanowires axis along the [0001] direction. The calculated Young modulus (65 GPa) is comparable to that of 1D ZnS nanosystems and three orders of magnitude lower than that of carbon fibers, suggesting that the modulus is dominated by the γ-MnS core. This was supported by bending and axial stress experiments, which showed that the strain is mostly confined to the γ-MnS core.

As a last application, we mention that 3–5 nm MnS NCs (a mixture of all three polymorphs) prepared inside mesoporous silica by impregnation/calcination were successfully used as a

catalyst for the growth of carbon nanocages when a flow of methane was passed on the NC-containing silica [55]. The latter have non-uniform size but their framework elements are 3–7 nm thick, consistent with the size of the MnS NCs. This suggests that the framework elements grow starting from the MnS NCs in the silica pores. A growth mechanism has been proposed involving the formation of reduced metal sites on the MnS NC surface where methane cracking occurs. The deposited carbon cannot form carbides and nucleates the growth of the nanocages. The authors claim that this is the first example of using a transition metal sulfide for the synthesis of carbon nanostructures.

7. Conclusions

We have reviewed the literature concerning the synthesis, properties, and application of MnS nanosystems having at least one dimension smaller than 100 nm, with a few exceptions regarding MnS sub-microparticles with interesting properties and applications. The wide variety of successful synthetic techniques for the preparation of 0D and 1D MnS nanosystems (both homogeneous and heterogeneous) with size, shape, and polymorphism control is astounding. However, the issue of independently controlling morphology and crystal structure is not yet completely solved. Further research in this direction is needed to foster application of MnS nanosystems in the above described fields. Recently, excellent results on the performance of MnS nanomaterials have been reported that we believe will further stimulate basic and applicative research in the exciting field of MnS nanosystems.

Author details

Anna M. Ferretti, Sara Mondini and Alessandro Ponti*

*Address all correspondence to: alessandro.ponti@istm.cnr.it

Laboratorio di Nanotecnologie, Istituto di Scienze e Tecnologie Molecolari, Consiglio Nazionale delle Ricerche, Milano, Italy

References

[1] Lokhande CD, Ennaoui A, Patil PS, Giersig M, Diesner K, Tributsch H. Process and characterisation of chemical bath deposited manganese sulphide (MnS) thin films. Thin Sol Films. 1998;330:70–75. doi: 10.1016/s0040-6090(98)00500-8

[2] Danielian A, Stevens KWH. Exchange interactions in the polymorphic forms of MnS. Proceedings of the Physical Society. 1961;77:124–128. doi: 10.1088/0370-1328/77/1/315

[3] Tappero R, Darco P, Lichanot A. Electronic structure of α-MnS (alabandite): An ab initio study. Chem Phys Lett. 1997;273:83–90. doi: 10.1016/s0009-2614(97)00591-5

[4] Hobbs D, Hafner J. Magnetism and magneto-structural effects in transition-metal sulphides. J Phys Condens Matter. 1999;11:8197–8222. doi: 10.1088/0953-8984/11/42/303

[5] Kravtsova AN, Stekhin IE, Soldatov AV, Liu X, Fleet ME. Electronic structure of MS (M=Ca,Mg,Fe,Mn): X-ray absorption analysis. Phys Rev B. 2004;69:134109, 12p. doi: 10.1103/PhysRevB.69.134109

[6] Viswanath R, Naik HSB, Kumar GSY, Kumar PNP, Harish KN, Prabhakara MC. Luminescence properties of blue-red emitting multilayer coated single structure ZnS/MnS/ZnS nanocomposites. Spectrochim Acta A. 2014;125:222–227. doi: 10.1016/j.saa.2014.01.022

[7] Zhang XV, Martin ST, Friend CM, Schoonen MAA, Holland HD. Mineral-assisted pathways in prebiotic synthesis: Photoelectrochemical reduction of carbon(+IV) by manganese sulfide. J Am Chem Soc. 2004;126:11247–11253. doi: 10.1021/ja0476415

[8] Chilton HM, Jackets SC, Hinson WH, Ekstrand K. Use of a paramagnetic substance, colloidal manganese sulfide, as an NMR contrast material in rats. J Nucl Med. 1984;25:604–607.

[9] Meng J, Zhao Y, Li Z, Wang L, Tian Y. Phase transfer preparation of ultrasmall MnS nanocrystals with a high performance MRI contrast agent. RSC Adv. 2016;6:6878–6887. doi: 10.1039/c5ra24775f

[10] Beltran-Huarac J, Palomino J, Resto O, Wang J, Jadwisienczak WM, Weiner BR, Morell G. Highly-crystalline γ-MnS nanosaws. RSC Adv. 2014;4:38103–38110. doi: 10.1039/c4ra05561f

[11] Beltran-Huarac J, Resto O, Carpena-Nunez J, Jadwisienczak WM, Fonseca LF, Weiner BR, Morell G. Single-crystal γ-MnS nanowires conformally coated with carbon. ACS Appl Mater Interfaces. 2014;6:1180–1186. doi: 10.1021/am404746k

[12] Lee SM, Lee J-K, Kang YC. Electrochemical properties of hollow-structured MnS-carbon nanocomposite powders prepared by a one-pot spray pyrolysis process. Chem. Asian J. 2014;9:590–595. doi: 10.1002/asia.201301261

[13] Ha D-H, Ly T, Caron JM, Zhang H, Fritz KE, Robinson RD. A general method for high-performance li-ion battery electrodes from colloidal nanoparticles without the introduction of binders or conductive-carbon additives: The cases of MnS, $Cu_{2-x}S$, and Ge. ACS Appl Mater Interfaces. 2015;7:25053–25060. doi: 10.1021/acsami.5b03398

[14] Tang Y, Chen T, Yu S. Morphology controlled synthesis of monodispersed manganese sulfide nanocrystals and their primary application in supercapacitors with high performances. Chem Commun. 2015;51:9018–9021. doi: 10.1039/c5cc01700a

[15] Chen T, Tang Y, Qiao Y, Liu Z, Guo W, Song J, Mu S, Yu S, Zhao Y, Gao F. All-solid-state high performance asymmetric supercapacitors based on novel MnS nanocrystal and activated carbon materials. Scientific Reports. 2016;6:23289, 9p. doi: 10.1038/srep23289

[16] Lu J, Qi PF, Peng YY, Meng ZY, Yang ZP, Yu WC, Qian YT. Metastable MnS crystallites through solvothermal synthesis. Chem Mater. 2001;13:2169–2172. doi: 10.1021/cm010049j

[17] Jun YW, Jung YY, Cheon J. Architectural control of magnetic semiconductor nanocrystals. J Am Chem Soc. 2002;124:615–619. doi: 10.1021/ja016887w

[18] Kan SH, Felner I, Banin U. Synthesis, characterization, and magnetic properties of α-MnS nanocrystals. Isr J Chem. 2001;41:55–61. doi: 10.1560/1FB3-1PF4-72JQ-0AQC

[19] Corliss L, Elliott N, Hastings J. Magnetic structures of the polymorphic forms of manganese sulfide. Phys Rev. 1956;104:924–928. doi: 10.1103/PhysRev.104.924

[20] Papp G. History of minerals, rocks and fossil resins discovered in the Carpathian region. Budapest: Hungarian Natural History Museum; 2004.

[21] Eriksson L, Kalinowski MP. $Mn_{1-x}Fe_xS$, $x \cong 0.05$, an example of an anti-wurtzite structure. Acta Crystallogr Sect E Struct Rep Online. 2001;57:I92–I93.

[22] Ma C, Beckett JR, Rossman GR. Browneite, MnS, a new sphalerite-group mineral from the Zaklodzie meteorite. Am Mineral. 2012;97:2056–2059.

[23] Pradhan N, Katz B, Efrima S. Synthesis of high-quality metal sulfide nanoparticles from alkyl xanthate single precursors in alkylamine solvents. J Phys Chem B. 2003;107:13843–13854.

[24] Tian L, Yep LY, Ong TT, Yi J, Ding J, Vittal JJ. Synthesis of NiS and MnS nanocrystals from the molecular precursors (TMEDA)M(SC{O}C_6H_5)$_{(2)}$ (M = Ni, Mn). Cryst Growth Des. 2009;9:352–357. doi: 10.1021/cg800536w

[25] Barry L, Copley M, Holmes JD, Otway DJ, Kazakova O, Morris MA. Synthesis and characterization of nanoparticulate MnS within the pores of mesoporous silica. J Solid State Chem. 2007;180:3443–3449. doi: 10.1016/j.jssc.2007.10.004

[26] Peng L, Shen S, Zhang Y, Xu H, Wang Q. Controllable synthesis of MnS nanocrystals from a single-source precursor. J Colloid Interface Sci. 2012;377:13-17. doi: 10.1016/j.jcis.2012.03.052

[27] Moloto N, Moloto MJ, Kalenga M, Govindraju S, Airo M. Synthesis and characterization of MnS and MnSe nanoparticles: Morphology, optical and magnetic properties. Opt Mater. 2014;36:31–35. doi: 10.1016/j.optmat.2013.06.023

[28] Li Z, Ji Y, Xie R, Grisham YS, Peng X. Correlation of CdS nanocrystal formation with elemental sulfur activation and its implication in synthetic development. J Am Chem Soc. 2011;133:17248–17256. doi: 10.1021/ja204538f

[29] Thomson JW, Nagashima K, Macdonald PM, Ozin GA. From sulfur-amine solutions to metal sulfide nanocrystals: Peering into the oleylamine-sulfur black box. J Am Chem Soc. 2011;133:5036–5041.

[30] Joo J, Na HB, Yu T, Yu JH, Kim YW, Wu FX, Zhang JZ, Hyeon T. Generalized and facile synthesis of semiconducting metal sulfide nanocrystals. J Am Chem Soc. 2003;125:11100–11105. doi: 10.1021/ja0357902

[31] Capetti E, Ferretti AM, Dal Santo V, Ponti A. Surfactant-controlled composition and crystal structure of manganese(II) sulfide nanocrystals prepared by solvothermal synthesis. Beilstein J Nanotech. 2015;6:2319–2329. doi: 10.3762/bjnano.6.238

[32] Puglisi A, Mondini S, Cenedese S, Ferretti AM, Santo N, Ponti A. Monodisperse octahedral α-MnS and MnO nanoparticles by the decomposition of manganese oleate in the presence of sulfur. Chem Mater. 2010;22:2804–2813. doi: 10.1021/cm903735e

[33] Tian Q, Tang M, Jiang F, Liu Y, Wu J, Zou R, Sun Y, Chen Z, Li R, Hu J. Large-scaled star-shaped α-MnS nanocrystals with novel magnetic properties. Chem Commun. 2011;47:8100–8102. doi: 10.1039/c1cc11621e

[34] Wang DS, Zheng W, Hao CH, Peng Q, Li YD. A synthetic method for transition-metal chalcogenide nanocrystals. Chem Eur J. 2009;15:1870–1875.

[35] An CH, Tang KB, Liu XM, Li FQ, Zhou G, Qian YT. Hydrothermal preparation of α-MnS nanorods from elements. J Cryst Growth. 2003;252:575–580. doi: 10.1016/s0022-0248(03)01001-7

[36] Zhang HT, Hyun BR, Wise FW, Robinson RD. A generic method for rational scalable synthesis of monodisperse metal sulfide nanocrystals. Nano Lett. 2012;12:5856–5860. doi: 10.1021/nl303207s

[37] Ma D, Huang S, Zhang L. One-pot synthesis and magnetic, electrical properties of single-crystalline α-MnS nanobelts. Chem Phys Lett. 2008;462:96–99. doi: 10.1016/j.cplett.2008.07.078

[38] Mu J, Gu Z, Wang L, Zhang Z, Sun H, Kang S-Z. Phase and shape controlling of MnS nanocrystals in the solvothermal process. J Nanopart Res. 2008;10:197–201. doi: 10.1007/s11051-007-9216-8

[39] Zhang C, Tao F, Liu GQ, Yao LZ, Cai WL. Hydrothermal synthesis of oriented MnS nanorods on anodized aluminum oxide template. Mater Lett. 2008;62:246–248. doi: 10.1016/j.matlet.2007.05.008

[40] Yang X, Wang Y, Wang K, Sui Y, Zhang M, Li B, Ma Y, Liu B, Zou G, Zou B. Polymorphism and formation mechanism of nanobipods in manganese sulfide nanocrystals induced by temperature or pressure. J Phys Chem C. 2012;116:3292–3297. doi: 10.1021/jp209591r

[41] Powell AE, Hodges JM, Schaak RE. Preserving both anion and cation sublattice features during a nanocrystal cation-exchange reaction: Synthesis of metastable wurtzite-type CoS and MnS. J Am Chem Soc. 2016;138:471–474. doi: 10.1021/jacs.5b10624

[42] Michel FM, Schoonen MAA, Zhang XV, Martin ST, Parise JB. Hydrothermal synthesis of pure α-phase manganese(II) sulfide without the use of organic reagents. Chem Mater. 2006;18:1726–1736. doi: 10.1021/cm048320v

[43] Kurz T, Chen L, Brieler FJ, Klar PJ, von Nidda HAK, Froeba M, Heimbrodt W, Loidl A. Minimal number of atoms to constitute a magnet: Suppression of magnetic order in spherical MnS nanoparticles. Phys Rev B. 2008;78:132408, 124p. doi: 13240810.1103/PhysRevB.78.132408

[44] Brieler FJ, Grundmann P, Froba M, Chen LM, Klar PJ, Heimbrodt W, von Nidda HAK, Kurz T, Loidl A. Formation of $Zn_{1-x}Mn_xS$ nanowires within mesoporous silica of different pore sizes. J Am Chem Soc. 2004;126:797–807. doi: 10.1021/ja038960j

[45] Zheng J, Yuan X, Ikezawa M, Jing P, Liu X, Zheng Z, Kong X, Zhao J, Masumoto Y. Efficient photoluminescence of Mn^{2+}ions in MnS/ZnS core/shell quantum dots. J Phys Chem C. 2009;113:16969–16974. doi: 10.1021/jp906390y

[46] Zheng J, Ji W, Wang X, Ikezawa M, Jing P, Liu X, Li H, Zhao J, Masumoto Y. Improved photoluminescence of MnS/ZnS Core/shell nanocrystals by controlling diffusion of Mn Ions into the ZnS shell. J Phys Chem C. 2010;114:15331–15336. doi: 10.1021/jp104513k

[47] Ge JP, Li YD. Controllable CVD route to CoS and MnS single-crystal nanowires. Chem Commun. 2003:2498–2499. doi: 10.1039/b307452h

[48] Ge JP, Wang J, Zhang HX, Li YD. A general atmospheric pressure chemical vapor deposition synthesis and crystallographic study of transition-metal sulfide one-dimensional nanostructures. Chem Eur J. 2004;10:3525–3530.

[49] Kim DS, Lee JY, Na CW, Yoon SW, Kim SY, Park J, Jo Y, Jung MH. Synthesis and photoluminescence of Cd-doped α-MnS nanowires. J Phys Chem B. 2006;110:18262–18266. doi: 10.1021/jp063965z

[50] Zhou J, Huang F, Xu J, Wang Y. $Cu_{1.94}S$-MnS dimeric nanoheterostructures with bifunctions: Localized surface plasmon resonance and magnetism. CrystEngComm. 2013;15:4217–4220. doi: 10.1039/c3ce00015j

[51] Gui YC, Qian LW, Qian XF. Hydrothermal synthesis of uniform rock salt (α-) MnS transformation from wurtzite (γ-) MnS. Mater Chem Phys. 2011;125:698–703. doi: 10.1016/j.matchemphys.2010.09.071

[52] Yang X, Wang Y, Sui Y, Huang X, Cui T, Wang C, Liu B, Zou G, Zou B. Size-controlled synthesis of bifunctional magnetic and ultraviolet optical rock-salt MnS nanocube superlattices. Langmuir. 2012;28:17811–17816. doi: 10.1021/la304228w

[53] Zhang N, Yi R, Wang Z, Shi R, Wang H, Qiu G, Liu X. Hydrothermal synthesis and electrochemical properties of α-manganese sulfide submicrocrystals as an attractive

electrode material for lithium-ion batteries. Mater Chem Phys. 2008;111:13–16. doi: 10.1016/j.matchemphys.2008.03.040

[54] Pearce CI, Pattrick RAD, Vaughan DJ. Electrical and magnetic properties of sulfides. Sulfide Mineral Geochem. 2006;61:127–180. doi: 10.2138/rmg.2006.61.3

[55] Barry L, Tobin J, Copley M, Holmes JD, Otway DJ, Morris MA. MnS doped mesoporous silica catalysts for the generation of novel carbon nanocages. Appl Catal A. 2008;341:8–11. doi: 10.1016/j.apcata.2007.12.008

[56] Xu G, Zhu YL, Ma XL. Cu2S nanowires and MnS/Cu2S nanojunctions derived from γ-MnS nanowires via selective cation-exchange reaction. Phys Status Solidi A. 2011;208:123–128. doi: 10.1002/pssa.201026124

IntechOpen